Linear cotangential transfers and safe orbits for elliptic orbit rendezvous

Peters, Thomas V.; Noomen, Ron

DOI
10.2514/1.G005152

Publication date
2021

Document Version
Accepted author manuscript

Published in
Journal of Guidance, Control, and Dynamics

Linear cotangential transfers and safe orbits for elliptic orbit rendezvous

Thomas V. Peters*
GMV, Tres Cantos, E-28760, Spain

Ron Noomen†
TU Delft, Delft, 2629 HS, The Netherlands

This article presents the theory for linear cotangential transfers and safe orbits for elliptic orbit rendezvous. Expressions for the transfer angle and the required ΔV's are derived. Singularities in the algorithm can occur if the two orbits intersect. Alternative maneuvers for such singular cases are developed. The linear cotangential transfer algorithm is compared to the non-linear cotangential transfer and the algorithm is found to be very similar. The development of the linear cotangential transfer leads to a new set of relative orbital elements that are well suited for defining safe trajectories. The characteristics of safe trajectories are discussed and a linear safety checking algorithm is developed. Finally, the combination of the cotangential transfers and safe orbits is used to define safe rendezvous trajectories for elliptical orbit rendezvous.

Nomenclature

a = *semi-major axis (m)*

$\boldsymbol{B}$ = *matrix of partial derivatives of the state vector to the orbital elements*

e = *eccentricity*

i = *inclination (°, rad)*

M = *mean anomaly (°, rad)*

n = *orbital rate (°/s, rad/s)*

* Project Manager, Space Segment & Robotics, GMV, Calle Isaac Newton 11, 28760 Tres Cantos, Spain.
† Assistant professor, Faculty of Aerospace Engineering, Delft University of Technology, Delft, the Netherlands.

r = *orbital radius (m)*

t = *time (s)*

$\boldsymbol{T}$ = *state vector transformation matrix*

T = *orbital period (s)*

$\boldsymbol{V}$ = *velocity vector (m/s)*

V = *orbital velocity (m/s)*

$\boldsymbol{x}$ = *state vector (m; m/s)*

α = *trajectory in-plane phase angle (°, rad)*

$\boldsymbol{\delta\alpha}$ = *relative orbital element vector*

$\boldsymbol{\Phi}$ = *state transition matrix*

φ = *transfer angle (°, rad)*

γ = *flight-path angle (°, rad)*

λ = *ratio of in-plane and out-of-plane oscillation*

ω = *argument of perigee (°, rad)*

Ω = *right ascension of the ascending node (°, rad)*

ϑ = *true anomaly (°, rad)*

τ = *trajectory phase angle (°, rad)*

I. Introduction

RENDEZVOUS and formation flying mission studies in recent years have been characterized by a greater drive towards on-board autonomy, and a desire to extend rendezvous capabilities to non-cooperative targets such as space debris. There is also an increasing interest in performing rendezvous and formation flying in elliptic orbits. These developments would extend the range of possible rendezvous missions from controlled, circular orbits with a cooperative target to uncontrolled, eccentric orbits with an uncooperative target.

Safe rendezvous trajectories are of great importance to mid-range rendezvous scenarios that feature limited navigation capabilities, limited ground contact opportunities, a high drive for on-board autonomy or a combination of these three. The mid-range rendezvous phase starts when the chaser switches from absolute navigation to relative navigation based on a camera sensor. The linear relative navigation problem based on angles-only navigation during the long-range phase is not fully observable unless maneuvers are performed [1] or individual features on the target can be distinguished [2]. To aid the angles-only navigation in achieving fast convergence, the relative trajectory of the chaser needs to include some variation in relative altitude with respect to the target. Some relative drift between the chaser and the target also improves performance of the navigation [3], as does the inclusion of the J_2 perturbation into the linear model [3] or the use of a non-linear approach [4], [5]. The Gauss [6] or Laplace method and a differential correction algorithm [7] could be used to initialize the filter, but ground tracking data can also be used to initialize the relative navigation filter [5]. The accuracy that can be achieved by means of ground tracking is lower than the accuracy that can be achieved by means of relative camera sensors [8], [9]. Passively safe, collision-free trajectories can facilitate the transition between ground-based tracking and relative navigation. Safe trajectories may also be required during the initial formation deployment and acquisition, or to return from non-nominal situations. For example, formation deployment based on eccentricity / inclination vector separation is proposed for the PROBA-3 mission [10], a precision formation flying mission in a highly eccentric orbit with eccentricity 0.81. In the case of PROBA-3, the relative sensors are only available at a relatively close range, such that the formation deployment and acquisition needs to be performed using maneuvers uploaded by ground command. The trajectory needs to remain safe for a longer period of time, because no on-board autonomy is present during this phase, and ground commands are expected to be available only once per day.

In a circular reference orbit scenario the Hohmann transfer and eccentricity / inclination vector separation [11] are considered important building blocks for constructing a guidance profile or reference trajectory for the mid-range rendezvous. The linear Hohmann transfer in circular orbit rendezvous is a transfer maneuver to an orbit with a different altitude for which the first and the second ΔV are equal in magnitude and direction [12]. A recent article describes how the eccentricity / inclination separation was used to define the trajectories for an un-cooperative rendezvous [13]. Both elements can be generalized for use in eccentric orbits, but there is some freedom in the choice of parameters or conditions that are kept invariant when the eccentricity is non-zero. The cotangential transfer is a generalization of the Hohmann transfer in circular orbit rendezvous. The condition that is kept invariant is the tangency at the initial and

terminal points. The generalization of eccentricity / inclination vector separation leads to families of collision-free relative trajectories when the eccentricity is larger than zero.

The non-linear cotangential transfer algorithm was developed in the early 1960's [14], but recently a new derivation of the algorithm has been presented [15]. The cotangential transfer is a type of transfer that is extremely useful for safe impulsive rendezvous. The cotangential transfer is near-optimal for transfers between elliptical orbits [16]. The transfer orbit has only a single intersection point with the terminal orbit, which enhances the safety of the transfer. Finally, the direction of the ΔV is tangential to the reference orbital velocity vector, which means that the spacecraft attitude can remain stationary in the tangential or flight-path reference frame, pointing in the general direction of the target. The ΔV for the cotangential transfer exceeds the ΔV of the optimal transfer by only 1% if the eccentricity is less than 0.2 [17]. A more extensive comparison shows that the cotangential transfer performs well over a wide range of true anomalies, if the orbits do not intersect [18]. If the orbits do intersect, singularities appear in the algorithm [19]. An iterative algorithm for linear, cotangential transfers between J_2 perturbed relative orbits is presented in [20]. An analytical algorithm for the linear cotangential transfer has been concisely described in [21] in the context of the development of a linear rendezvous guidance system. Another description of linear cotangential transfers is provided in [22], but the solution for the transfer angle is not provided.

The problem of optimal formation reconfiguration has been addressed in several recent papers [23], [24], [25]. Gaias and D'Amico [23] provide maneuvering schemes for circular orbits and identifies the cotangential transfer case that is currently studied as the tangent-tangent bi-impulsive maneuver with zero or non-zero difference in semi-major axis. If the relative semi-major axis is zero, the solution is identified as requiring numerical solution of the transfer angle, and if the relative semi-major axis is non-zero, the solution is identified as requiring numerical solution of both the location of the first maneuver *and* the transfer angle. Gaias and D'Amico [23] also provide lower bounds for the ΔV for formation reconfigurations in circular orbits. Chernick and D'Amico [24], [25] extend the analysis of the lower bounds for the ΔV for formation reconfigurations in eccentric orbits and provide maneuvering schemes based on reachable set theory. Lower bounds for the ΔV and a three-impulse maneuver scheme are provided by Chernick and D'Amico [24]. Gaias and D'Amico [23] and Chernick and D'Amico [24] point out that bi-impulsive maneuvering schemes generally must be solved numerically, and cannot achieve the absolute ΔV minimum because they lack extra degrees of freedom to allow optimization of the ΔV. Closed form expressions for bi-impulsive maneuvers have been used in flight demonstrations in near circular orbits. These closed-form bi-impulsive maneuver solutions can only

establish three desired ROE after execution [24]. In the relative motion problem the out-of-plane coordinate is decoupled from the in-plane motion and can be controlled separately. Chernick and D'Amico [24], [25] provide a maneuvering scheme for the out-of-plane motion.

Linear relative motion theories can be derived either by solving the linearized equations of relative motion [26], or by finding the matrices of partial derivatives of the orbital elements to the Cartesian state [27], [28]. The equivalence of both approaches can be demonstrated [29]. For circular orbit rendezvous the equations that describe the relative motion are known as the Clohessy-Wiltshire or Hill-Clohessy-Wiltshire equations [30]. These equations can be recast in terms of relative orbital elements [31]. Relative motion theories that include perturbations can be obtained relatively easily from (semi-)analytical satellite theories. The state transition matrix is often generated for use in differential correction orbit determination schemes [27], [32]. Gim and Alfriend derived a relative motion theory that includes J_2 from Brouwer's theory [33]. An overview of different state transition matrices is provided by Alfriend et al [34]. Recent work provides a number of methods for including J_2 and drag for short-term and long-term propagation [35], [36], [37], [38]. Note that theories that include J_2 and drag apply to central bodies that possess an equatorial bulge and an atmosphere, such as the Earth. The perturbation due to J_2 is of the order of J_2, times the mean orbital rate, times the propagation time, or $O(10^{-3})$ for transfer durations of about half an orbit in low Earth orbit. Relative drag can have a major impact on the long-term evolution of relative trajectories, and it depends on multiple factors such as the ambient density, orbital velocity and the ratio of the ballistic coefficients of the chaser and the target. In this article it is assumed that the ballistic coefficients of the chaser and the target are comparable in magnitude, and that relative drag is negligible. Perturbations are excluded in this analysis of guidance algorithms, because maneuvers are expected to occur frequently during the rendezvous, and thrust errors can be as large as a few percent of the nominal ΔV [39]. Thrust errors can have out-of-plane components, and for this reason safe trajectories such as the eccentricity / inclination vector separation are designed to take into account margins for these and other perturbations. Guidance algorithms based on unperturbed relative motion can still be used even if the perturbations are not negligible or the propagation time is long. In such cases guidance strategies that divide the guidance problem into long-term evolution and short-term maneuvering can be applied in a scheme referred to as precompensation [24]. In this scheme the long-term evolution model (which includes J_2, drag and other perturbations) is used to plan a sequence of changes in the relative orbital elements. These changes in the relative orbital elements are realized by means of impulsive ΔV's that

are planned for a short time interval of up to a few revolutions during which the effect of the perturbations is negligible, and the impulsive ΔV's are calculated using the unperturbed relative motion model.

This article presents a novel set of algorithms for cotangential transfer maneuvers and trajectories that can be used for rendezvous problems in eccentric orbits. An important driver in the development of the algorithms presented in this article has been to try to link the theory of elliptic rendezvous to elementary treatments of circular orbit rendezvous, such that rendezvous in elliptic orbits can be seen as a straightforward extension of circular orbit rendezvous. Many elementary discussions are available for circular orbit rendezvous and most aspects of these treatments can directly be applied to elliptic orbits when suitable assumptions are made. In this paper the relative dynamics are described using linearized relative motion around an unperturbed, eccentric Keplerian orbit to ensure that the connection with maneuvers developed for linearized relative motion around an unperturbed, circular Keplerian orbit (the Clohessy Wiltshire equations) is as clear as possible. A previous article detailed the development of an analytical algorithm for non-drifting transfers that can be compared to the radial hop trajectory in circular orbit rendezvous [40]. The present article discusses the cotangential transfer and eccentricity / inclination vector separation [11] (also referred to as the projected circular orbit [34]) as the basic building blocks of a rendezvous strategy for elliptic orbit rendezvous. These two concepts seem unrelated at first sight but a deep connection exists between the two upon closer investigation. This connection is exploited to develop a set of related algorithms that taken together can be used to design a rendezvous strategy. The cotangential transfer maneuver presented in this article is a closed-form bi-impulsive in-plane transfer solution that can establish the desired relative semi-major axis, eccentricity and argument of perigee. The solution presented in this paper provides the transfer angle if the location of the first maneuver is given, and is valid for eccentric orbits. Intersecting initial and final trajectories can cause singularities in the linear cotangential maneuver computation algorithm, and the singularities occur at the intersection points. Seen in another way, the study of the singularities in the linear cotangential maneuver algorithm reveals a connection with trajectory safety features. Specifically, a linear trajectory crossing algorithm can be derived from the cotangential transfer algorithm [41]. The present article shows that the trajectory crossing algorithm can be used not only to reveal the singularities in the cotangential transfer, but also to establish short-term in-plane trajectory safety and to generalize the eccentricity / inclination vector separation to eccentric orbits. The development of the cotangential transfer algorithm leads to a new set of relative orbital elements (ROE) that can be used to define these families of relative

trajectories that generalize the eccentricity / inclination vector separation. Appendix B provides the relationship between the ROE defined in this paper and other sets of ROE [26], [28].

This paper is the result of an investigation into the operational aspects of the cotangential transfer algorithm. Section II provides a brief description of the linearized motion model. Section III provides the full derivation and a comprehensive analysis of the linear cotangential transfer algorithm, to examine singularities in the algorithm and to develop maneuvers for the singular case. Section IV defines families of relative trajectories that generalize the eccentricity / inclination vector separation strategy based on relative orbital elements (ROE) that follow naturally from the derivation of the cotangential transfer and to examine the safety of these families of trajectories. Section V develops a rendezvous strategy based on the cotangential transfer and the eccentricity / inclination vector separation generalized to eccentric orbits. The novel contribution of this investigation is a set of algorithms for cotangential maneuver computation, safe orbit definition and rendezvous trajectory design that generalize circular orbit rendezvous design concepts and as such simplify the design of elliptic orbit rendezvous trajectories.

II. Linearized Relative Motion Model

The orbit of the target spacecraft is taken as the reference orbit. The reference orbit is assumed to be an unperturbed elliptical Keplerian orbit for the purpose of developing the maneuvering scheme. Figure 1 shows the local vertical, local horizontal (LVLH) and the tangential or flight-path (TAN) reference frames. The Cartesian state vector is defined as $\mathbf{x} = [x \quad y \quad z \quad \dot{x} \quad \dot{y} \quad \dot{z}]^T$. A subscript is used to indicate whether the relative state is in the LVLH frame or in the TAN frame. Because the principal focus of this analysis is aimed at non-equatorial, eccentric orbits (far away from the singularities at e = 0 and i = 0), the familiar Keplerian orbital elements are used to define the vector of ROE as $\boldsymbol{\delta\alpha} = [\delta a \quad \delta e \quad \delta i \quad \delta\Omega \quad \delta\omega \quad \delta M]^{\mathrm{T}}$.

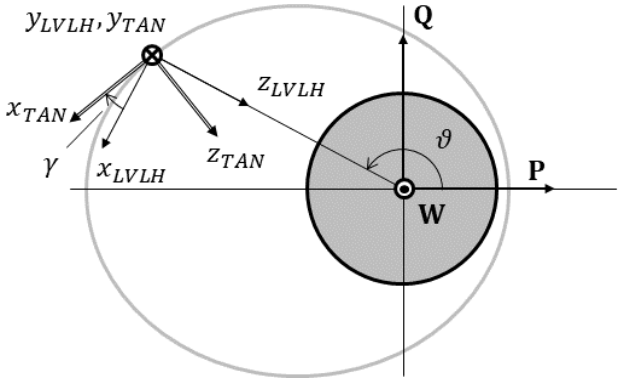

Fig. 1 LVLH and TAN frames with respect to the perifocal frame.

The derivation of the state transition matrix in terms of the Keplerian elements is provided by Montenbruck and Gill [27] for relative motion in the inertial frame and by Schaub and Junkins [28] for relative motion in the LVLH frame and is not repeated here. The details of the transformation and the mapping matrices for the TAN frame coordinates are given in Appendix A. In a linearized setting the cotangential transfer is based on two impulses parallel to the velocity vector of the reference orbit. The general expression for a two-pulse maneuver is given by Gaias and D'Amico [23] and Chernick and D'Amico [24]:

$$\boldsymbol{\delta\alpha}^{+}(t_2) = \boldsymbol{\Phi}_{\alpha}(t_2, t_1)\left\{\boldsymbol{\delta\alpha}^{-}(t_1) + \boldsymbol{\Gamma}_{LVLH}(t_1)\mathbf{R}_{\gamma}(t_1)\boldsymbol{\Delta V}_{TAN.1}\right\} + \boldsymbol{\Gamma}_{LVLH}(t_2)\mathbf{R}_{\gamma}(t_2)\boldsymbol{\Delta V}_{TAN,2} \tag{1}$$

The superscripts "+" and "-" indicate the state vector immediately before and immediately after the application of a ΔV. The matrix $\boldsymbol{\Gamma}$ is the control-input matrix or Gauss' variational equations in matrix form. The rotation matrix $\mathbf{R}_{\gamma}$ indicates a rotation around the y-axis by flight-path angle γ, see also Appendix A.

III. Linear Cotangential Transfer

A. Cotangential Transfer Problem Solution

The first step in developing the linear cotangential transfer algorithm is to write Eq. (1) explicitly in terms of the cotangential impulses and the ROE. Battin [42] provides expressions for Gauss' variational equations for the Keplerian elements and for components of the ΔV along the velocity vector and perpendicular to it. The perpendicular component of the ΔV is dropped and only the column of the matrix is used which relates the parallel component of the ΔV to changes in the ROE.

$$\begin{bmatrix} \delta a_2^{+} \\ \delta e_2^{+} \\ \delta \omega_2^{+} \\ \delta M_2^{+} \end{bmatrix} = \begin{bmatrix} 1 & 0 & 0 & 0 \\ 0 & 1 & 0 & 0 \\ 0 & 0 & 1 & 0 \\ -\frac{3}{2}a^{-1}n(t_2 - t_1) & 0 & 0 & 1 \end{bmatrix} \left(\begin{bmatrix} \delta a_1^{-} \\ \delta e_2^{-} \\ \delta \omega_1^{-} \\ \delta M_1^{-} \end{bmatrix} + \frac{2}{eV_1} \begin{bmatrix} a\eta^{-2} e\theta_1^2 \\ (\rho_1 - \eta^2) \\ \sin\vartheta_1 \\ -\rho_1^{-1}(\rho_1 + e^2)\eta \sin\vartheta_1 \end{bmatrix} \Delta V_{\parallel,1} \right) + \frac{2}{eV_2} \begin{bmatrix} a\eta^{-2} e\theta_2^2 \\ (\rho_2 - \eta^2) \\ \sin\vartheta_2 \\ -\rho_2^{-1}(\rho_2 + e^2)\eta \sin\vartheta_2 \end{bmatrix} \Delta V_{\parallel,2} \tag{2}$$

where η is equal to $\sqrt{1-e^2}$, $\rho = 1 + e\cos\vartheta$, $\theta = \sqrt{2\rho - \eta^2}$, and n is the orbital rate. The expression for the local orbital velocity appearing in the matrix in equation (2) can be derived from the vis-viva law [6]:

$$V = an\eta^{-1}\theta \tag{3}$$

The scaling functions ρ and θ, which govern the behavior of the orbital radius and the orbital velocity, respectively, form part of many expressions that are derived in this article. The equations for the relative semi-major axis, eccentricity and argument of perigee are required for the solution of the transfer angle, while the equation for the relative mean anomaly is required to find the along-track motion during the transfer. The first three equations can be simplified to:

$$\begin{aligned} a^{-1}\Delta a &= a^{-1}(\delta a_2^+ - \delta a_1^+) = \eta^{-2}\theta_1^2 \Delta V_{\parallel,1}^* + \eta^{-2}\theta_2^2 \Delta V_{\parallel,2}^* \\ e\Delta e &= e(\delta e_2^+ - \delta e_1^+) = (\rho_1 - \eta^2)\Delta V_{\parallel,1}^* + (\rho_2 - \eta^2)\Delta V_{\parallel,2}^* \\ e\Delta\omega &= e(\delta\omega_2^+ - \delta\omega_1^+) = \sin\vartheta_1\, \Delta V_{\parallel,1}^* + \sin\vartheta_2\, \Delta V_{\parallel,2}^* \end{aligned} \tag{4}$$

The velocity impulses have been normalized according to $\Delta V^* = 2V^{-1}\Delta V$. The solution strategy is as follows. First, the transfer angle is found as a function of the initial true anomaly and the differences in relative semi-major axis, eccentricity and argument of perigee. Second, the velocity impulses are found. Finally, the equation for the relative mean anomaly is used to determine the along-track distance after the maneuver. To solve Eq. (4) the system is rewritten as:

$$\begin{aligned} a^{-1}\Delta a - 2\eta^{-2} e\Delta e &= \Delta V_{/\!/,1}^* + \Delta V_{/\!/,2}^* \\ e(a^{-1}\Delta a - 2\eta^{-2} e\Delta e) - \Delta e &= -\cos\vartheta_1\, \Delta V_{/\!/,1}^* - \cos\vartheta_2\, \Delta V_{/\!/,2}^* \\ e\Delta\omega &= \sin\vartheta_1\, \Delta V_{/\!/,1}^* + \sin\vartheta_2\, \Delta V_{/\!/,2}^* \end{aligned} \tag{5}$$

The left-hand sides of these equations are functions of the ROE only, and not of the true anomaly. This means that these elements are ROE in their own right. To define the new set, Eq. (5) is multiplied by the semi-latus rectum. The left-hand-side of the first of Eq. (5) can now be compared to the variation of the semi-latus rectum $\delta p = \eta^2\delta a - 2ae\delta e$ [28]. The new relative orbital elements replacing the relative semi-major axis, eccentricity and argument of perigee (and their inverse relations) are defined as follows:

$$\begin{aligned} C_1 &= \delta p = \eta^2\delta a - 2ae\delta e & \delta a &= \eta^{-4}\big((1+e^2)C_1 - 2eC_2\big) \\ C_2 &= e\delta p - p\delta e & \delta e &= p^{-1}(eC_1 - C_2) \\ C_3 &= -ep(\delta\omega + \cos i\, \delta\Omega) & \delta\omega &= -e^{-1}p^{-1}C_3 \end{aligned} \tag{6}$$

The term $\cos i\, \delta\Omega$ has been added to the definition of C_3 to decouple the in-plane and out-of-plane motion, see Appendix B. For in-plane transfers such as the cotangential transfer, there is no change in the right ascension of the ascending node Ω such that $\Delta C_3 = ep\,\Delta\,\omega$ for in-plane transfers.

Eq. (5) can be rewritten using angle sum identities for ϑ_2 to yield a set of equations in terms of the initial true anomaly, the transfer angle φ and the scaled velocity impulses. The transfer angle φ is the difference between the initial true anomaly and the final true anomaly.

$$\begin{aligned}
\Delta C_1 &= p\left(\Delta V_{\parallel,1}^* + \Delta V_{\parallel,2}^*\right) \\
\Delta C_2 &= p\left(-\cos\vartheta_1\,\Delta V_{\parallel,1}^* - \cos\vartheta_1\cos\varphi\,\Delta V_{\parallel,2}^* - \sin\vartheta_1\sin\varphi\,\Delta V_{\parallel,2}^*\right) \\
\Delta C_3 &= p\left(-\sin\vartheta_1\,\Delta V_{\parallel,1}^* - \sin\vartheta_1\cos\varphi\,\Delta V_{\parallel,2}^* - \cos\vartheta_1\sin\varphi\,\Delta V_{\parallel,2}^*\right)
\end{aligned} \tag{7}$$

After elementary manipulation of these equations the following result is obtained:

$$\begin{aligned}
\Delta C_1 + \cos\vartheta_1\,\Delta C_2 + \sin\vartheta_1\,\Delta C_3 &= p\Delta V_{/\!/,2}^*(1-\cos\varphi) \\
\sin\vartheta_1\,\Delta C_2 - \cos\vartheta_1\,\Delta C_3 &= p\Delta V_{/\!/,2}^*\sin\varphi
\end{aligned} \tag{8}$$

The left-hand sides of this equation are real-valued trigonometric polynomials of the initial true anomaly with the new ROE as coefficients. The polynomials are labeled P_1 and P_2. P_1 (i.e., a ΔP_1) depends on C_1, C_2 and C_3, while P_2 only depends on C_2 and C_3.

$$\begin{aligned}
P_1 &= C_1 + C_2\cos\vartheta_1 + C_3\sin\vartheta_1 \\
P_2 &= C_2\sin\vartheta_1 - C_3\cos\vartheta_1
\end{aligned} \tag{9}$$

Eq. (8) now becomes:

$$\begin{aligned}
\Delta P_1 &= p\Delta V_{/\!/,2}^*(1-\cos\varphi) \\
\Delta P_2 &= p\Delta V_{/\!/,2}^*\sin\varphi
\end{aligned} \tag{10}$$

The solution for the transfer angle can be found by performing the Weierstrass substitution, and is given by:

$$\varphi = 2\tan^{-1}\left(\frac{\Delta P_1}{\Delta P_2}\right) \tag{11}$$

Care should be taken when ΔP_2 is equal to 0 as the argument of the arctangent function becomes infinitely large; in this case the transfer angle is equal to 180°. Next, the velocity impulses are determined. Squaring Eq. (10) and summing them leads to the following expression for the second velocity impulse (where it is noted that Eq. (10) is used twice to obtain the expression for ΔP_1 and simplify the result):

$$\Delta V_{/\!/,2}^* = \frac{1}{2}\frac{(\Delta P_1)^2+(\Delta P_2)^2}{p\Delta P_1} \tag{12}$$

To find the simplest possible expressions for the ΔV's, note that the sum of the squares of polynomials P_1 and P_2 is equal to:

$$(\Delta P_1)^2 + (\Delta P_2)^2 = (\Delta C_s)^2 + 2\Delta C_1 \Delta P_1 \tag{13}$$

To simplify expressions the parameter C_s is defined by:

$$(\Delta C_s)^2 = (\Delta C_2)^2 + (\Delta C_3)^2 - (\Delta C_1)^2 \tag{14}$$

This means that the second velocity impulse can also be written as:

$$\Delta V^*_{/\!/,2} = \frac{1}{p}\left\{\frac{1}{2}\frac{(\Delta C_s)^2}{\Delta P_1} + \Delta C_1\right\} \tag{15}$$

Using the first of Eq. (7) a simple expression for the normalized velocity impulses can be found:

$$\begin{aligned} \Delta V^*_{/\!/,1} &= -\frac{(\Delta C_s)^2}{2p\Delta P_1} \\ \Delta V^*_{/\!/,2} &= \frac{1}{p}\Delta C_1 - \Delta V^*_{/\!/,1} \end{aligned} \tag{16}$$

This completes the derivation of the cotangential transfer algorithm. In this derivation the ROE C_1, C_2, C_3 and C_s have been defined. The ROE C_1, C_2 and C_3 are alternatives to the semi-major axis, eccentricity and argument of perigee. The constant C_s does not form part of this new set. The set of alternative elements is completed by defining element C_4 based on the mean anomaly. Chernick and D'Amico [24] and Riggi and D'Amico [43] refer to this orbital element as the modified relative mean longitude. In the current treatment the modified relative mean longitude is scaled by $a \cdot \eta^{-1}$:

$$C_4 = a(\delta\omega + \cos i\, \delta\Omega + \eta^{-1}\delta M) \tag{17}$$

The C set of ROE is non-singular when the eccentricity goes to zero, and can be seen as a generalization of the travelling ellipse formulation that is in use in circular orbit rendezvous, see Appendix B. Using this new element the equation for the relative mean anomaly from Eq. (2) can be rewritten as follows:

$$\Delta C_4 = -\frac{3}{2}\eta^{-1} n(t_2 + kT)\delta a 1 — \frac{3}{2}\eta^{-3} an(t_2 - t_1 + kT)\theta_1^2 \Delta V^*_{\parallel,1} - ae\sin\vartheta_1\, \rho_1^{-1}\Delta V^*_{\parallel,1} - ae\sin\vartheta_2\, \rho_2^{-1}\Delta V^*_{\parallel,2}, \quad k \in \mathbb{Z} \tag{18}$$

Allowance has been made for a coasting arc in the initial orbit and a longer coasting time in the transfer orbit, where the coasting time in the transfer orbit can be extended by integer multiples of the orbital period. In principle it would be possible to solve this equation for the initial true anomaly. However, like Kepler's equation, this equation does not have a closed-form solution, and a numerical method would need to be used. In section V an alternative approach is used to ensure that the chaser arrives at the correct along-track distance.

The ΔV required for the linear cotangential maneuver can be compared to the ΔV lower bounds provided by Chernick and d'Amico [24]. Chernick and d'Amico [24] show that a lower bound for the ΔV can be established that is based on the ROE that requires the largest ΔV to change, and this ROE change is referred to as the dominant ROE change. The lower bound for in-plane transfers is given by the largest of the ΔV's required to change the semi-major axis, the modified relative mean longitude and the eccentricity vector.

$$(na\eta)^{-1}\Delta V_{LB} = \max\left(\frac{a^{-1}\|\Delta\delta a\|}{2(1+e)}, \frac{\|\Delta\delta\lambda_e\|}{3(1+e)\Delta M}, \frac{\|\Delta\delta\mathbf{e}\|}{\sqrt{3e^4-7e^2+4}}\right) \tag{19}$$

In equation (19), $a\eta\delta\lambda_e = C_4$ and the relative eccentricity vector is given by [28]:

$$\delta\mathbf{e} = \begin{bmatrix}\delta q_1\\ \delta q_2\end{bmatrix} = \begin{bmatrix}\cos\omega & -e\sin\omega\\ \sin\omega & e\cos\omega\end{bmatrix}\begin{bmatrix}\delta e\\ \delta\omega\end{bmatrix} \tag{20}$$

The ΔV required for the linear cotangential maneuver can be solved for the special case of co-apsidal transfers to compare expressions for the case of dominant $\|\Delta\delta a\|$ and dominant $\|\Delta\delta\mathbf{e}\|$. The cotangential maneuver (like the Hohmann transfer in circular orbit rendezvous) is not designed for solving changes in the modified relative mean longitude, and the case of dominant $\|\Delta\delta\lambda_e\|$ is not considered for comparison here. The total ΔV for the general linear cotangential transfer is given by:

$$\Delta V_{tot} = \Delta V_{\parallel,1} + \Delta V_{\parallel,2} = \frac{1}{2}an\eta^{-1}\left\{\theta_1\left\|\frac{(\Delta C_s)^2}{2p\Delta P_1}\right\| + \theta_2\left\|\frac{1}{p}\Delta C_1 + \frac{(\Delta C_s)^2}{2p\Delta P_1}\right\|\right\} \tag{21}$$

If the change in the relative argument of perigee is equal to zero, and the transfer is started at apogee or at perigee, then the transfer angle is 180° and the ΔV can be rewritten in terms of changes in the relative semi-major axis and relative eccentricity.

$$\Delta V_{tot} = \begin{cases}\frac{1}{2}n\{\eta\Delta\delta a - ae\eta^{-1}\Delta\delta e\}, & \frac{-(1-e)\eta^2}{2-2e-\eta^2} < \frac{a\Delta\delta e}{\Delta\delta a} < \frac{(1+e)\eta^2}{2+2e-\eta^2}\\ \frac{1}{2}na\eta^{-1}\Delta\delta e, & \frac{a\Delta\delta e}{\Delta\delta a} \le \frac{-(1-e)\eta^2}{2-2e-\eta^2} \vee \frac{a\Delta\delta e}{\Delta\delta a} \ge \frac{(1+e)\eta^2}{2+2e-\eta^2}\end{cases} \tag{22}$$

The nature of the total ΔV changes depending on whether the initial and final orbit intersect or not. The limit cases can be derived from the control input matrix (explicitly given in equation (2)), determining the ratio of the change in semi-major axis and the change in eccentricity that can be achieved by means of a single impulse. Intersecting initial and final orbits are further discussed in section III.C.

If the cotangential maneuver only changes the semi-major axis, then the total ΔV is related to the lower bound as:

$$\frac{\Delta V_{tot}}{\Delta V_{LB}} = \frac{\frac{1}{2}n\eta\Delta\delta a}{\frac{n\eta}{2(1+e)}\Delta\delta a} = 1 + e \tag{23}$$

Equation (23) shows that the ΔV is higher than the lower bound by a factor equal to the eccentricity. The lower bound is obtained by examining the effect of a single, tangential maneuver performed at perigee. Such a maneuver achieves the maximum change in semi-major axis, but it also changes the eccentricity. This is a strong indication that the ΔV lower bound for dominant $\|\Delta\delta a\|$ is unlikely to be achievable.

On the other hand, if the cotangential maneuver changes the eccentricity and the change in eccentricity is larger than the limits identified in (22), then the total ΔV is related to the lower bound as:

$$\frac{\Delta V_{tot}}{\Delta V_{LB}} = \frac{\frac{1}{2}na\eta^{-1}\Delta\delta e}{\frac{na\eta\Delta\delta e}{\sqrt{3e^4-7e^2+4}}} = \frac{1}{2}\eta^{-2}\sqrt{3e^4 - 7e^2 + 4} \tag{24}$$

Equation (24) shows that the total ΔV is less than 4.1% above the lower bound if the eccentricity of the reference orbit is smaller than 0.5, and less than 11.4% above the lower bound if the eccentricity of the reference orbit is smaller than 0.7.

B. Geometrical Representation of the Transfer

The cotangential transfer can be represented geometrically in terms of the C set of ROE and the normalized velocity impulses in a diagram. This diagram is a phase portrait of the scaled z-coordinate in the TAN frame and facilitates the identification of key points and relevant angles in the transfer problem. The geometrical representation provides a direct connection between the key ROE C_1, C_2 and C_3, and the behavior of the z-coordinate in the tangential frame. It ensures that the phase angles of the transfer trajectory can be identified by inspection, and it allows for a straightforward identification of the singularities in the algorithm as crossing points with the reference trajectory. The tangency condition at the end of the trajectory can be verified in the diagram in Fig. 2 as the transfer ends at zero altitude (z = 0) with zero vertical velocity (z' = 0). The diagram therefore captures all important geometrical features of coplanar elliptic trajectories with respect to a reference orbit.

First note that the z-coordinate in the TAN frame can be expressed as (see Appendix B):

$$\rho\theta z_{TAN} = -(C_1 + C_2\cos\vartheta + C_3\sin\vartheta) = -P_1 \tag{25}$$

The z-coordinate depends on the same polynomial P_1 that was identified in the solution of the cotangential transfer angle, Eq. (9). The z-coordinate is scaled by ρ and by θ as follows:

$$\hat{z}_{TAN} = \rho\theta z_{TAN} = \frac{V\eta^3}{nr} z_{TAN} \tag{26}$$

In other words, the scaling depends both on the local orbital velocity and on the local orbital radius. The rate of change of the scaled coordinate with respect to the true anomaly is given by:

$$\hat{z}'_{TAN} = \frac{d}{d\vartheta}\hat{z}_{TAN} = -\frac{d}{d\vartheta}P_1 = P_2 \tag{27}$$

The behavior of the scaled z-coordinate is affected by tangential velocity impulses and it has been shown in Eq. (25) that a simple relation exists between the scaled z-coordinate and the C set of ROE. The effect of the normalized tangential and radial velocity impulses on the C set of ROE is derived from Eq. (1) and (6) (see also Appendix B):

$$\frac{\partial \mathbf{c}}{\partial \mathbf{V}^*_{TAN}} = p\begin{bmatrix} 1 & e\sin\vartheta\,\rho^{-1} \\ -\cos\vartheta & \frac{1}{2}(1+e^2)\sin\vartheta\,\rho^{-1} \\ -\sin\vartheta & -\frac{1}{2}\{2e+(1+e^2)\cos\vartheta\}\rho^{-1} \\ -e\sin\vartheta\,\rho^{-1}\eta^{-2} & \eta^{-2} \end{bmatrix} \tag{28}$$

The effect of a normalized tangential velocity impulse on the elements C_1, C_2 and C_3 is expressed in terms of simple trigonometric functions. To complete the diagram, define the parameter C_m and the phase angle α as follows:

$$\begin{aligned} C_m &= \sqrt{(C_2)^2 + (C_3)^2} \\ \alpha &= \tan^{-1}(C_3, C_2) \end{aligned} \tag{29}$$

The geometry of the cotangential transfer can now be summarized in a diagram. Figure 2 shows the geometry of a generic cotangential transfer.

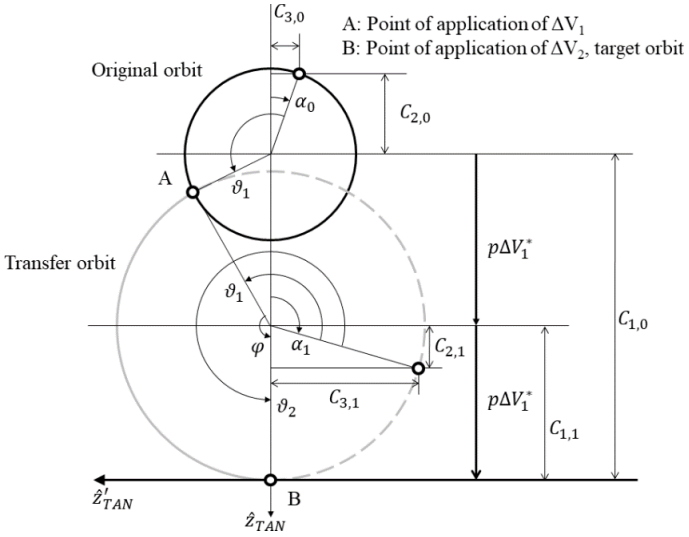

Fig. 2 Cotangential transfer diagram.

The transfer starts in the relative orbit represented by the circle at the top, parameterized by the three ROE $C_{1,0}$, $C_{2,0}$ and $C_{3,0}$. The scaled z-coordinate traces out a circle in the phase portrait diagram, with a phase angle α determined by the relative magnitudes of the ROE C_2 and C_3. A tangential velocity impulse changes the altitude of the circle of the scaled z-coordinate and the ROE C_2 and C_3 change in such a way as to match the derivative of the scaled z-coordinate at the point of application. The z-coordinate now traces out a circular arc equal to the transfer angle φ to reach the target orbit. The transfer arc is indicated by the set of ROE $C_{1,1}$, $C_{2,1}$ and $C_{3,1}$. The second tangential velocity impulse ends the transfer at the origin. The scaled z-coordinate in the TAN frame with respect to an elliptic reference orbit behaves in a manner similar to the z-coordinate in the LVLH frame with respect to a circular orbit. The scaled z-coordinate in the TAN frame follows a simple harmonic oscillation around a fixed mean altitude and it is independent of the modified relative mean longitude. All these aspects are the same as the behavior of the z-coordinate in the LVLH frame in circular orbit rendezvous.

C. Singularities in the Algorithm and Alternative Maneuvers

The cotangential algorithm contains singularities for certain sets of initial and final conditions. Inspection of the cotangential transfer diagram for the singular cases shows that singularities in the cotangential transfer algorithm occur when the initial orbit intersects the final orbit. Figure 3 shows this situation in the cotangential transfer diagram. The shaded region in Fig. 3 represents the portion of the trajectory below the reference orbit, with the intersections occurring at S_1 and S_2. This diagram allows determining of the location of the singularities, namely, the true anomalies of the intersection points. Intersections occur when the scaled z-coordinate can become zero. By inspection of Fig. 3 and Eq. (25) the intersection criterion is deduced, namely that the absolute value of ΔC_1 needs to be smaller than ΔC_m. The true anomalies of the intersections can be found by finding the zeros of Eq. (25).

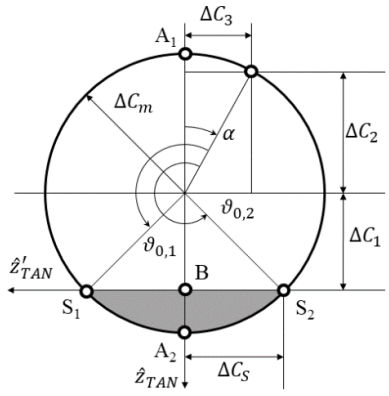

Fig. 3 Location of singularities in the cotangential transfer algorithm.

The geometrical relations of Fig. 3 can be analyzed to help find the solution for the true anomalies of the intersections:

$$\begin{aligned} \sin\vartheta_{0,1} &= -\frac{\Delta C_2\Delta C_s+\Delta C_1\Delta C_3}{(\Delta C_m)^2}, \quad \cos\vartheta_{0,1} = \frac{\Delta C_3\Delta C_s-\Delta C_1\Delta C_2}{(\Delta C_m)^2} \\ \sin\vartheta_{0,2} &= \frac{\Delta C_2\Delta C_s-\Delta C_1\Delta C_3}{(\Delta C_m)^2}, \quad \cos\vartheta_{0,2} = -\frac{\Delta C_3\Delta C_s+\Delta C_1\Delta C_2}{(\Delta C_m)^2} \end{aligned} \tag{30}$$

The behavior of the cotangential transfer algorithm near the singularity can be understood graphically by comparing Fig. 2 and Fig. 3, approaching the singularity from below or above. In both cases, the algorithm fits a circle of infinite radius through the point S and point B, and as the center of the circle of the transfer orbit moves further away from the target orbit the ΔV increases. When approaching the singularity from above the transfer angle approaches 0 as the true anomaly approaches the true anomaly of the intersection. When approaching the singularity from below the transfer angle approaches 2π as the true anomaly approaches the true anomaly of the intersection. If the orbits intersect the first and the second ΔV are in opposite directions, while if the orbits do not intersect (as depicted in Fig. 2) both ΔV's are in the same direction. The first condition of Eq. (7) still applies, which states that for linearized dynamics the sum of the normalized ΔV's needs to be equal to the change in semi-latus rectum. If the ΔV's have opposite sign, then they can become unbounded, while if the ΔV's have the same sign, then the first condition of Eq. (7) provides an upper limit to the size of each of the ΔV's. Clearly, the singularity in the algorithm needs to be avoided to limit the ΔV. Three alternatives to the cotangential transfer are explored when the initial and final orbit intersect.

The first option is to perform the transfer from points that are as far removed from the singularity as possible, starting either above (1) or below (2) the target orbit. In Fig. 3 these points are labelled A_1 and A_2. The ΔV's have opposite sign even if the transfer starts as far from the singularity as possible. The transfer angle φ is equal to 180°. The transfer for case 1 is developed below. The transfer for case 2 can be developed in an analogous manner. Eq. (16) shows that the ΔV depends on the polynomial P_1. At point A the polynomial P_1 becomes:

$$\Delta P_{1,\alpha} = \Delta C_1 + \Delta C_2\cos\alpha + \Delta C_3\sin\alpha = \Delta C_1 + \Delta C_m \tag{31}$$

This expression is inserted into Eq. (16) to obtain the normalized ΔV's:

$$\begin{aligned} \Delta V^*_{\parallel,1,\alpha} &= \frac{1}{2}p^{-1}(\Delta C_1 - \Delta C_m) \\ \Delta V^*_{\parallel,2,\alpha} &= \frac{1}{2}p^{-1}(\Delta C_1 + \Delta C_m) \end{aligned} \tag{32}$$

The second option is to use a single maneuver performed at the crossing point. The ΔV needs to satisfy the following equation:

$$\begin{bmatrix}\Delta C_1\\ \Delta C_2\\ \Delta C_3\end{bmatrix}+p\begin{bmatrix}1 & e\sin\vartheta\,\rho^{-1}\\ -\cos\vartheta & \frac{1}{2}(1+e^2)\sin\vartheta\,\rho^{-1}\\ -\sin\vartheta & -\frac{1}{2}\{2e+(1+e^2)\cos\vartheta\}\rho^{-1}\end{bmatrix}\begin{bmatrix}\Delta V_{\parallel}^*\\ \Delta V_{\perp}^*\end{bmatrix}=\begin{bmatrix}0\\0\\0\end{bmatrix} \tag{33}$$

This equation can be solved by inserting the true anomaly of one of the two crossing points from Eq. (30), and solving the overdetermined system. Alternatively, it can be observed that the tangential component of the ΔV needs to nullify the difference in semi-major axis; only the tangential component of the ΔV can change the semi-major axis. The tangential ΔV is found to be equal to:

$$\Delta V_{/\!/}^* = \frac{\eta^2}{\theta^2}\left(\frac{\delta a^+ - \delta a^-}{a}\right) \tag{34}$$

The ΔV is rewritten in terms of the C set of ROE:

$$p\Delta V_{/\!/}^* = \frac{\eta^2}{\theta^2}\left(\frac{(1+e^2)\Delta C_1 - 2e\Delta C_2}{\eta^2}\right) = \frac{(1+e^2)\Delta C_1 - 2e\Delta C_2}{\theta^2} \tag{35}$$

The radial ΔV can be found by inserting the tangential ΔV into the first line of Eq. (33) and solving for the radial component. (Of course, line two and three lead to the same result.)

$$p\Delta V_{\perp}^* = \frac{\rho\left(\Delta C_1 - p\Delta V_{/\!/}^*\right)}{e\sin\vartheta} = \frac{2\rho}{\theta^2}\frac{\cos\vartheta\Delta C_1 - \Delta C_2}{\sin\vartheta} \tag{36}$$

The true anomaly of the first intersection from Eq. (30) is inserted to find the radial ΔV at this point:

$$\frac{\cos\vartheta_{0,1}\Delta C_1 - \Delta C_2}{\sin\vartheta_{0,1}} = -\frac{(\Delta C_2\Delta C_S + \Delta C_1\Delta C_3)\Delta C_S}{\Delta C_2\Delta C_S + \Delta C_1\Delta C_3} = -\Delta C_S \tag{37}$$

The radial component of the ΔV at the first intersection is equal to:

$$p\Delta V_{\perp}^* = -\frac{2\rho_{0,1}}{\theta_{0,1}^2}\Delta C_S \tag{38}$$

At the second crossing the radial component switches sign; the tangential component of the ΔV is the same as for the first crossing. This maneuver is performed at the intersection point, which achieves the desired change in relative orbital elements with a single impulse. This means that transfer is optimal under the assumption that a single ΔV is used.

For the third alternative there is only a single point of intersection (so $\Delta C_m = \Delta C_1$). The tangential ΔV to be applied at the intersection point can be found by means of Eq. (35). The intersection occurs at $\vartheta = \pi + \alpha$, so, using the definition of α from Eq. (29) and the fact that $C_m = \Delta C_1$, Eq. (35) can be rewritten as:

$$\Delta V_{/\!/}^{*} = \frac{1}{p}\Delta C_1 \tag{39}$$

This means that a tangential impulse at the single point of intersection that is aimed to remove the semi-major axis is basically the same as the second maneuver of the cotangential transfer, and therefore also corrects the relative eccentricity and argument of perigee.

$$\cos\vartheta = -\operatorname{sgn}(\Delta C_1)\frac{\Delta C_2}{\Delta C_s},\ \sin\vartheta = -\operatorname{sgn}(\Delta C_1)\frac{\Delta C_3}{\Delta C_s} \tag{40}$$

The formulation for the crossing maneuver cannot be simplified as readily for specific cases as the cotangential maneuver. The crossing maneuver can achieve the desired set of ROE in a single impulse, but the same change can be achieved more efficiently in a multi-impulse scheme. To show this, consider the following example comparing the ΔV for the cotangential transfer and the crossing maneuver to the lower bound. Assume the target spacecraft is orbiting in a reference orbit around Earth with a semi-major axis of 20000 km and an eccentricity of 0.2. The chaser performs the following change in relative orbital elements:

$$\Delta\boldsymbol{\delta\alpha} = [\Delta\delta a \quad \Delta\delta e \quad \Delta\delta\omega] = [200\,m \quad 1\cdot 10^{-5} \quad 0°] \tag{41}$$

Equation (22) states that if the change in relative eccentricity is larger than $8 \cdot 10^{-6}$, then the initial and final relative orbits intersect, and the change in relative eccentricity dominates. For this transfer the change in parameter C_1 is -208 m, the change in parameter C_2 is -233.6 m, and the change in C_3 is zero. Equation (19) is used to find the lower bound for the ΔV as 22.7 mm/s, and equation (22) is used to find the ΔV for the cotangential transfer from perigee to apogee as 22.8 mm/s, or 0.5% above the lower bound. Using equation (30) the two crossings are found to be symmetric with respect to apogee, and occur at a true anomaly of 48.7° and 311.3°. According to equations (35) and (38) the ΔV to be applied at the crossing has a magnitude of 35.6 mm/s, or 56.9% above the lower bound. This example illustrates that the cotangential maneuver, performed far away from the singularities at the crossing points, is generally more efficient in terms of ΔV than the crossing maneuver if the cotangential maneuver is performed far away from the intersection points.

D. Comparison with Non-Linear Cotangential Transfer Solution

The non-linear coplanar cotangential transfer problem can be stated as follows: Given the semi-major axes, eccentricities and arguments of perigee of the initial and final orbits and the true anomaly at which the transfer starts, find the transfer angle of the transfer orbit. The orbital parameters of the transfer orbit and the transfer time can then easily be calculated. This derivation follows Zhang [15], [44], with some modifications. The derivation starts from the following relationship between the terminal radii, flight-path angles and the transfer angle given in [45 p. 240].

$$r_2 \tan\gamma_1 + r_1 \tan\gamma_2 = (r_2 - r_1)\cot\frac{1}{2}\varphi \tag{42}$$

The first step to solve Eq. (42) is to multiply by $\rho_1\rho_2$ and by $\tan\frac{1}{2}\varphi$ to remove the devisors:

$$(p_1 e_2 \sin\vartheta_2 + p_2 e_1 \sin\vartheta_1)\tan\frac{1}{2}\varphi = p_2\rho_1 - p_1\rho_2 \tag{43}$$

Unlike [15], the departure point or initial true anomaly is considered as given, such that the unknowns in equation (43) are the transfer angle and the true anomaly of the arrival point. The transfer angle is defined as the difference in true latitude, that is, $\varphi = \omega_2 - \omega_1 + \vartheta_2 - \vartheta_1$. The transfer angle is used to eliminate the true anomaly of the arrival point:

$$\{p_1 e_2 \sin(\vartheta_1 - \Delta\omega + \varphi) + p_2 e_1 \sin\vartheta_1\}\tan\frac{1}{2}\varphi = p_2(1 + e_1\cos\vartheta_1) - p_1\{1 + e_2\cos(\vartheta_1 - \Delta\omega + \varphi)\} \tag{44}$$

Then angle sum and difference operations on the sine and cosine terms of the compound angle can be performed, followed by the Weierstrass substitution on the sine and cosine terms of the transfer angle φ. Simplification leads to the following expression for the transfer angle:

$$\tan\frac{\varphi}{2} = \frac{p_2 - p_1 + (p_2 e_1 - p_1 e_2\cos\Delta\omega)\cos\vartheta_1 - p_1 e_2 \sin\Delta\omega\sin\vartheta_1}{(p_2 e_1 - p_1 e_2\cos\Delta\omega)\sin\vartheta_1 + p_1 e_2\sin\Delta\omega\cos\vartheta_1} \tag{45}$$

In equation (45) the following expressions for the ROE C_1, C_2 and C_3 can be identified that are the non-linear counterpart to the definition in Eq. (6):

$$\begin{aligned}
\Delta C_{1,nl} &= \Delta p = p_2 - p_1 \\
\Delta C_{2,nl} &= p_1 e_1(1 - \cos\Delta\omega) + e_1\Delta p - p_1\Delta e\cos\Delta\omega = p_2 \mathrm{e}_1 - p_1 e_2\cos\Delta\omega \\
\Delta C_{3,nl} &= -p_1(e_1\sin\Delta\omega + \Delta e\sin\Delta\omega) = -p_1 e_2\sin\Delta\omega
\end{aligned} \tag{46}$$

Eq. (45) can now be written in the same form as Eq. (11), the only difference being that non-linear analogues of the parameters C_1, C_2 and C_3 are used:

$$\varphi = 2\tan^{-1}\left(\frac{\Delta P_{1,nl}}{\Delta P_{2,nl}}\right) \tag{47}$$

The singularities in the algorithm are the same as those given by Eq. (30). To show this, the condition for intersection is examined. The intersection can be found by letting the radius of the initial orbit be equal to radius of the second orbit, and solving for the true anomaly of the initial orbit.

$$\frac{p_1}{1+e_1\cos(l-\omega_1)} = \frac{p_2}{1+e_2\cos(l-\omega_2)} \tag{48}$$

The true longitude l is equal to $\vartheta_1 + \omega_1$, so the following equation can be found from Eq. (48):

$$p_1 + p_1 e_2\cos(\vartheta_1 - \Delta\omega) = p_2 + p_2 e_1\cos\vartheta_1 \tag{49}$$

Using the cosine difference formula and collecting terms in the sine and cosine of the true anomaly of the first orbit leads to the following expression:

$$p_2 - p_1 + (p_2 e_1 - p_1 e_2\cos\Delta\omega)\cos\vartheta_1 - p_1 e_2\sin\Delta\omega\sin\vartheta_1 = \Delta C_{1,nl} + \Delta C_{2,nl}\cos\vartheta_1 + \Delta C_{3,nl}\sin\vartheta_1 = 0 \tag{50}$$

This is indeed the non-linear equivalent of setting Eq. (25) to zero.

The determination of the non-linear ROE C_1, C_2 and C_3 shows that this set of ROE is defined with respect to a certain reference orbit, unlike the set of Kepler elements. These ROE show up in the determination of whether orbits intersect and the determination of the required tangential ΔV's to transfer between orbits. In the linear case, the new ROE can be also be used as alternatives to the classical ROE to simplify the description of the relative motion in the TAN frame. The fact that there is a close correspondence between the linear and the non-linear cotangential transfer means that the orbit intersection checks and the identification of the correct initial true anomaly for the cotangential transfer between intersecting orbits from section III.C can be used in the case of non-linear transfers as well. This approach was followed in [46] to create a non-linear guidance function for the long-range rendezvous phase of an MSR type mission.

IV. Trajectory Safety and Safe Orbits

Trajectory safety is an important design consideration, especially in the presence of trajectory uncertainty. Along-track uncertainty tends to be much larger than the uncertainty in the radial and cross-track directions, because small errors in the estimation of the semi-major axis lead to uncertainty in mean anomaly that grows with time due to the coupling between these elements [11]. The eccentricity / inclination vector separation strategy was developed to

exploit this fact; eccentricity vector separation leads to a separation in the radial direction and inclination vector separation leads to a separation in the cross-track direction. If the angle between the relative eccentricity vector and the relative inclination vector (or, alternatively, the phase angle between the radial and cross-track oscillations) is selected properly, then the trajectory remains collision-free even in the presence of trajectory uncertainty.

A. Eccentric Safe Orbits from Generalized Inclination / Eccentricity Vector Separation

Eccentricity / inclination vector separation is a strategy used in circular reference orbits to define trajectories that are safe from collisions. The resulting trajectory is referred to as eccentricity / inclination vector separation, projected circular orbit or safe orbit if the in-plane and out-of-plane oscillations have the same amplitude. In this document the name "safe orbit" will be used. The eccentricity / inclination vector separation strategy is used for collocating geostationary communications satellites [47] and has recently been used in several formation flying missions in low Earth orbit [48], [49], [50] .The reason this type of trajectory is safe is that the projection on the y-z plane of the LVLH frame can be shaped such that the chaser never comes close to the origin. If the amplitudes of the in-plane and out-of-plane oscillations are equal, the projection on the y-z plane is a circle. The center of the circle always lies on the z-axis, but it can have a certain non-zero altitude with respect to the origin. If the altitude is not equal to zero, then the trajectory experiences some along-track drift.

The concept of the safe orbit is generalized to eccentric reference orbits. Trajectories are discussed in a general setting first and a phase angle is included to shift from safe to other types of trajectories such as the halo formation [47]. The specific case of non-drifting safe orbits is treated. Finally, a method is derived to generate safe orbits that pass through a specified point at a specified true anomaly of the reference orbit. Specific geometric conditions at particular points along the orbit are of interest, for example, for satisfying geometric constraints such as ground station visibility, illumination conditions or alignment with astronomical objects. Target observation by means of visual cameras could for example be performed from a safe orbit if the Sun-target-chaser geometry is favorable.

Jiang et al [51] show that drift-free relative trajectories in the LVLH frame lie on a quadric surface in three-dimensional space, and that the quadric surface can be a one-sheet hyperboloid, an elliptic cone or an elliptic cylinder. The idea of embedding the rather complicated relative trajectory into a simpler geometric shape is very interesting. Instead of examining a single trajectory, the whole family of trajectories that lie on the surface can be examined at once. The geometric shape of the surface is simpler, so the analysis to determine whether the shape satisfies certain constraints (such as the trajectory being free from collisions) becomes simpler. If the entire shape satisfies the

constraint, then the analysis can stop after this first step. If it does not, then the more complex geometry of the individual trajectory can be analyzed to determine whether that specific trajectory at least satisfies the constraint. The approach of Jiang et al [51] cannot be applied directly to generate general safe trajectories because Jiang et al [51] do not include the semi-major axis difference (and therefore trajectory drift) into the analysis. The analysis is performed in the LVLH frame, and the LVLH z-coordinate is dependent on the relative mean anomaly which makes the LVLH z-coordinate dependent on the along-track drift if the relative semi-major axis is non-zero. In other words, if along-track drift is present, then the principal assumption in Jiang et al [51] is violated and the simple geometrical relations identified by Jiang et al no longer apply. Dang et al in [52], [53] base their analysis on the work of Jiang et al [51] and provide analytical bounds on the inter-satellite distance, but their approach does not retain the simplicity of the geometrical bounds provided by Jiang et al [51]. In this section geometrical relations are sought that are similar to those found by Jiang et al [51] and that enable fast analysis of families of trajectories. The TAN frame is used instead of the LVLH frame, and simple geometrical relations are defined between the elements C and families of trajectories in the TAN frame. This allows for a straightforward definition of safe orbits that generalize the concept of eccentricity / inclination vector separation, and for simple and fast checks of the trajectory safety. The focus lies on the perpendicular and out-of-plane coordinates, and safe orbits are defined in such a way that the larger uncertainty in the along-track direction does not influence the overall safety of the trajectory, similar to the approach in [11] for circular orbit rendezvous.

In section III.B it has been observed that the z-coordinate in the TAN frame is independent of the modified relative mean longitude and that the behavior of the scaled z-coordinate is a simple trigonometric function. In the following sections the idea to identify simple geometries for trajectory families is applied to identify safe trajectories in the TAN frame. Because the z-coordinate in the TAN frame is independent of the modified relative mean longitude, only the projection on the y-z plane needs to be examined to determine whether the possibility of a collision exists or not. This means that the number of dimensions that need to be analyzed in the first step of the analysis is reduced from 3 to 2. Both the y-coordinate and the z-coordinate in the TAN frame are fairly simple trigonometric functions of the true anomaly, and no secular terms are present. The collision analysis becomes correspondingly simpler.

B. General Trajectories and Safe Orbits

The out-of-plane motion is parameterized in terms of the elements C_5 and C_6, which relate to the relative orbital elements δi and $\delta\Omega$ as follows:

$$C_5 = -p(\cos\omega\,\delta i + \sin i \sin\omega\,\delta\Omega)$$
$$C_6 = p(\sin\omega\,\delta i - \sin i \cos\omega\,\delta\Omega) \tag{51}$$

To fully decouple the in-plane and out-of-plane motion the in-plane element C_3 is redefined as $C_3 = -ep(\delta\omega + \cos i\,\delta\Omega)$. The out-of-plane coordinate in the TAN frame can be expressed as a function of C_5 and C_6:

$$\hat{y}_{TAN} = \rho y_{TAN} = C_5 \sin\vartheta - C_6 \cos\vartheta \tag{52}$$

In equation (52) $\hat{y}_{TAN}$ is the out-of-plane coordinate scaled by ρ. Next Eq. (25) is reparametrized using Eq. (29) and Eq. (52) is re-parameterized using the following definitions:

$$C_5 = \lambda C_m \cos\beta\,,\ C_6 = \lambda C_m \sin\beta \tag{53}$$

The parameter λ is the ratio of the amplitude of the out-of-plane oscillation with respect to the amplitude of the in-plane oscillation and β is the true anomaly at which the chaser crosses the orbital plane of the target in ascending direction (i.e., the relative ascending node). Note that the oscillation in the out-of-plane direction can also be inverted by changing the sign of the elements C_5 and C_6. The scaled motion in the y-z plane of the TAN frame can now be written in the following form:

$$\hat{y}_{TAN} = \lambda C_m \sin(\vartheta - \beta) = \lambda C_m \sin(\tau - \tau_0)$$
$$\hat{z}_{TAN} = -\{C_1 + C_m \cos(\vartheta - \alpha)\} = -\{C_1 + C_m \cos\tau\} \tag{54}$$

In equation (54) $\tau = \vartheta - \alpha$ and $\tau_0 = \beta - \alpha$. For non-zero C_m and λ the scaled coordinates in the y-z plane traces a line if τ_0 is equal to ½π, a circle if τ_0 is equal to 0 and λ = 1 and an ellipse otherwise. The case of τ_0 equal to 0 is of interest for generalizing the safe orbit to an eccentric reference orbit. Of course many different generalizations of the projected circular orbit are now possible that all approach a circular projection when the eccentricity goes to zero, due to the presence of the amplitude ratio λ. That is to say, one could assign whichever function of the eccentricity to the parameter λ, as long as it approaches to 1 when the eccentricity goes to zero. If no restrictions are placed on the amplitude ratio, then the parameter λ can be set to any value. Equation (54) indicates that if $|C_1| < |C_m \cos\tau_0|$, the trajectories wind around the origin.

One-parameter families of curves can now be identified that depend on the parameter α and that have the same value for the parameters C_1, C_m, λ and τ_0. The parameter α is a phase angle, C_1 is the relative altitude, C_m the dimension or size, λ the ratio of amplitudes of the out-of-plane to the in-plane oscillations and τ_0 the angle between the relative eccentricity and inclination vectors. For the definition of eccentricity / inclination vector separation with a circular

reference orbit similar parameters are used. In case of a circular reference orbit the in-plane phase angle α can be varied without altering the shape of the relative trajectory: the projection of the trajectory on the x-z plane of the LVLH frame remains a 2:1 ellipse, and the projection of the trajectory on the y-z plane remains a circle (only if λ is equal to 1, of course). In the case of an elliptic reference orbit the shape of trajectories is more complicated because of the scaling factors acting on the y and z coordinates, and each member of the family of trajectories is scaled differently. On the other hand, the boundary of a family of trajectories as a whole (defined by means of Eq. (54) in terms of the parameters C_1, C_m, λ and τ_0) is reasonably simple. The boundary can be obtained by examining the envelope of the family of curves parameterized by τ and the extreme values of the scaling function ρ. The point of the boundary closest to the origin always lies on the ellipse for which ρ is equal to 1 + e, that is to say, the closest approach of the trajectory family as a whole always occurs at perigee, because in this case both the y and z coordinates are scaled by the largest value. The closest approach of the family evaluated at perigee therefore provides a conservative, lower bound estimate of the closest approach of any individual member of that family.

Following this general discussion the eccentricity / inclination vector separation is examined. Eccentricity / inclination vector separation occurs when τ0 is equal to 0. If τ_0 is equal to 0, then the scaled coordinates behave as follows:

$$\begin{aligned} \hat{y}_{TAN} &= \lambda C_m \sin\tau \\ \hat{z}_{TAN} &= -(C_1 + C_m \cos\tau) \end{aligned} \tag{55}$$

This is the parametric equation of an ellipse with center (0,-C_1), major axis C_m along the z-axis and minor axis λ· C_m along the y-axis. Figure 4 shows the families of safe orbits that Eq. (55) generates. The value of the parameter λ is 1, C_m is equal to 10. On the left of Fig. 4 C_1 = 0 and on the right C_1 = C_m. The scaled coordinates (that is, y is scaled by ρ and z is scaled by ρθ) are the same for all members of the trajectory family.

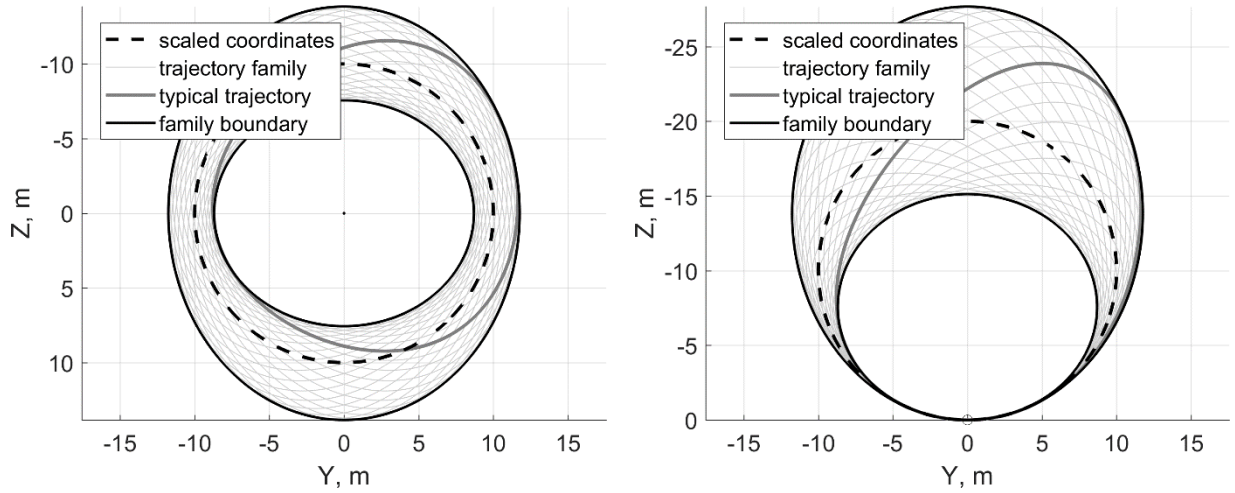

(a) $C_1 = 0$ **(b) $C_1 = C_m$**

Fig. 4 Boundaries for safe trajectories.

Figure 4 shows that the inner boundary of the family of trajectories around the origin is determined by the inner elliptical boundary that results from $\rho = 1 + e$ if $|C_1| < |C_m|$. This family of trajectories encloses the origin and contains both drifting and non-drifting trajectories. To ensure drift-free trajectories, the difference in semi-major axis must be equal to zero. In terms of the ROE C_1 and C_2 this means:

$$C_1 = \frac{2e}{1+e^2} C_2 = \frac{2e}{1+e^2} C_m \cos\alpha \tag{56}$$

The drift-free safe orbit encloses the origin. Finally, for drift-free trajectories centered on the origin $C_4 = 0$.

The safe orbit formulation in this article can be compared to the formulations of the eccentricity / inclination vector separation found in literature. D' Amico and Montenbruck [11] define the eccentricity / inclination vector separation using the eccentricity vector and the inclination vector. In near-circular orbits the eccentricity vector is usually parameterized in terms of small differences in the parameters $q_1 = e\cos\omega$ and $q_2 = e\sin\omega$ [28], and the inclination vector is parameterized in terms of δi and $\delta\Omega\sin i$. The ROE defining the eccentricity and inclination vectors are multiplied by the argument of latitude $u = \vartheta + \omega$. The elements C can be recovered from the elements used by Chernick and D'Amico [24] using:

$$\begin{bmatrix} C_1 \\ C_2 \\ C_3 \\ C_4 \\ C_5 \\ C_6 \end{bmatrix} = p \begin{bmatrix} 1 & 0 & -2\eta^{-2} e\cos\omega & -2\eta^{-2} e\sin\omega & 0 & 0 \\ e & 0 & -\eta^{-2}(1+e^2)\cos\omega & -\eta^{-2}(1+e^2)\sin\omega & 0 & 0 \\ 0 & 0 & \sin\omega & -\cos\omega & 0 & -e\cot i \\ 0 & \eta & 0 & 0 & 0 & 0 \\ 0 & 0 & 0 & 0 & -\cos\omega & -\sin\omega \\ 0 & 0 & 0 & 0 & \sin\omega & -\cos\omega \end{bmatrix} \begin{bmatrix} a^{-1}\delta a \\ \delta\lambda_e \\ \delta q_1 \\ \delta q_2 \\ \delta i \\ \delta\Omega\sin i \end{bmatrix} \tag{57}$$

The formulation in terms of elements C conveniently decouples the in-plane and out-of-plane motions. The main difference with the formulation for circular orbits is that the semi-latus rectum is used as the basis for elements C_1 and C_2.

C. Trajectories with Alignment

This section discusses trajectories that pass through a user-specified position vector in the TAN frame at a specified true anomaly. This can be useful for example for ensuring proper lighting conditions of the target spacecraft. The relative semi-major axis δa, the amplitude ratio λ and the out-of-plane phase angle τ_0 are given as design parameters. The y and z coordinates of the trajectory are given as a function of C_2 and C_3 by Eq. (54). The value of C_1 in the equation for the z-coordinate as a function of C_2 and the relative semi-major axis can be obtained from equation (6).

$$C_1 = \left(1 + e^2\right)^{-1}\left(\eta^4 \delta a_{des} + 2eC_2\right) \tag{58}$$

The equations for the y- and z-coordinate can then be written as the following system of equations:

$$\begin{bmatrix} y_{TAN} \\ z_{TAN} + \rho^{-1}\theta^{-1}\frac{\eta^4}{1+e^2}\delta a_{des} \end{bmatrix} = \rho^{-1}\theta^{-1}\begin{bmatrix} \lambda\theta\sin(\vartheta-\tau_0) & -\lambda\theta\cos(\vartheta-\tau_0) \\ -\left(\frac{2e}{1+e^2}+\cos\vartheta\right) & -\sin\vartheta \end{bmatrix}\begin{bmatrix} C_2 \\ C_3 \end{bmatrix} \tag{59}$$

The solution for this system of equations is:

$$\begin{bmatrix} C_2 \\ C_3 \end{bmatrix} = \rho\left\{\cos\tau_0 + \frac{2e}{1+e^2}\cos(\vartheta-\tau_0)\right\}^{-1} \times \begin{bmatrix} \lambda^{-1}\sin\vartheta & -\theta\cos(\vartheta-\tau_0) \\ -\lambda^{-1}\left(\frac{2e}{1+e^2}+\cos\vartheta\right) & -\theta\sin(\vartheta-\tau_0) \end{bmatrix}\begin{bmatrix} y_{TAN} \\ z_{TAN} + \rho^{-1}\theta^{-1}\frac{\eta^4}{1+e^2}\delta a_{des} \end{bmatrix} \tag{60}$$

The constant C_4 is obtained from the x-coordinate in the tangential frame, which is given by (Appendix B):

$$x_{TAN} = \rho^{-1}\eta^{-2}\theta^{-1}\{e(\theta^2+2)\sin\vartheta\, C_1 - 2(\rho+e^2)\sin\vartheta\, C_2 + 2(e+\cos\vartheta)\rho C_3\} + \theta C_4 \tag{61}$$

The constant C_1 as a function of C_2 and the relative semi-major axis is inserted, and the equation is solved:

$$C_4 = \theta^{-1}x_{TAN} - \eta^2\theta^{-2}\frac{e\sin\vartheta}{\rho}\left(\frac{2}{1+e^2}\rho + 1\right)\delta a_{des} + 2\theta^{-2}\left(\frac{\sin\vartheta}{1+e^2}C_2 - \frac{e+\cos\vartheta}{\eta^2}C_3\right) \tag{62}$$

Finally, the elements C_5 and C_6 are found from:

$$\begin{aligned} C_5 &= \lambda(C_2\cos\tau_0 - C_3\sin\tau_0) \\ C_6 &= \lambda(C_2\sin\tau_0 + C_3\cos\tau_0) \end{aligned} \tag{63}$$

The procedure to obtain a trajectory that passes through a point (x, y, z) in the TAN frame, with the relative semi-major axis δa, the amplitude ratio λ and the out-of-plane phase angle τ_0 given as design parameters, is as follows. First, Eq. (60) is used to obtain C_2 and C_3. Eq. (58) is used to obtain C_1 and Eq. (62) is used to obtain C_4. Finally, Eq. (63) is used to obtain the elements C_5 and C_6. The state in the TAN frame can be found using the matrices defined in Appendix B. Alternatively, the C set of ROE can be converted to Keplerian ROE.

Some limitations of this procedure need to be pointed out. The procedure obviously does not work if the amplitude ratio λ is set to zero, because in this case the relative motion occurs in the orbital plane of the reference orbit. Second, if the out-of-plane phase angle τ_0 is smaller than $\sin^{-1}\left(\frac{2e}{1+e^2}\right)$, then the divisor in Eq. (60) can become zero for certain values of the true anomaly, which leads to singular trajectories that may have infinite size.

V. Rendezvous Strategy Based on Cotangential Transfers and Safe Orbits

In this section an example of a rendezvous strategy is presented that incorporates the ideas developed in the previous sections. Perturbations are excluded from this analysis. The perturbation-free maneuvering strategy described here can be incorporated into a guidance function that does consider perturbations using the precompensation technique described by Chernick and D'Amico [24].

The initial conditions for the rendezvous strategy are a drift orbit at a given altitude below the target orbit. The terminal conditions for the strategy are a safe orbit with specific properties, namely, arriving at a specific point at a specific true anomaly. Tangential and out-of-plane maneuvers are used to reach the terminal conditions. Figure 5 shows a diagram of the rendezvous strategy.

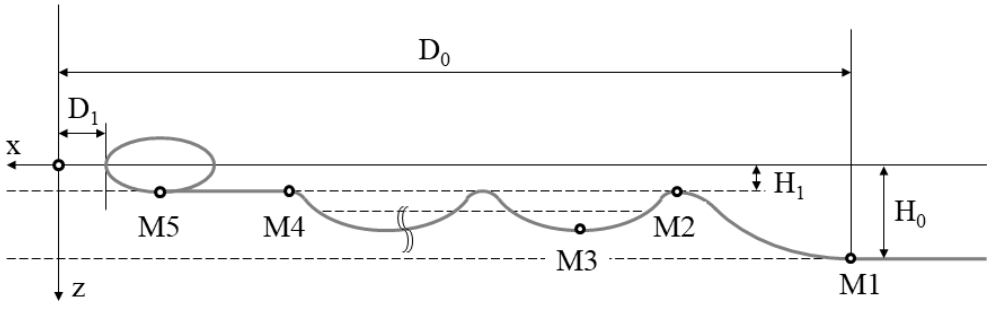

Fig. 5 Rendezvous strategy.

Before maneuver M1 the chaser is a co-elliptic orbit below the target orbit. Maneuver M1 is a cotangential transfer that raises the relative apogee to H_1. Between maneuvers M2 and M4 the chaser is in a drifting orbit with a relative perigee below H1. The drift orbit with altitude variations ensures that the chaser arrives at the proper distance from

the target when performing maneuver M4. Maneuver M3 is an out-of-plane maneuver. Maneuver M4 inserts the chaser into a co-elliptic orbit. Finally, maneuver M5 inserts the chaser into a safe orbit. To complete the definition of this strategy, two additional aspects need to be examined. First, the lowest possible co-elliptic drift orbit that connects to the safe orbit needs to be found. This co-elliptic orbit is tangent to the safe orbit. In addition, the drift rate between M2 and M4 needs to be modulated to ensure proper phasing.

A. Co-elliptic Orbits Connecting to Safe Orbits

A co-elliptic orbit is defined with respect to a reference orbit. It is coplanar with the reference orbit and has the same argument of perigee. The value of the eccentricity is such that the altitude variation with respect to the reference orbit is as small as possible [54]. The linear co-elliptic orbit is defined in terms of the ROE as follows:

$$\delta e = -e\mathrm{a}^{-1}\delta a,\ \delta\omega = 0 \tag{64}$$

The co-elliptic orbit in terms of the parameters C_1, C_2 and C_3 is found from equation (6). The equation for the z coordinate in the co-elliptic orbit can now be found from equations (6), (25) and (64):

$$z_{TAN} = -\rho^{-1}\theta\delta a = -\frac{1}{\cos\gamma}\delta a \tag{65}$$

The range of the z-coordinate of the co-elliptic orbit is determined by the flight path angle. At apogee and at perigee, the flight path angle is zero and $z_{TAN} = -\delta a$. The maximum flight path angle occurs at $\vartheta = \cos^{-1}(-e)$, and at this point the z-coordinate reaches its extremum $z_{TAN} = -\eta^{-1}\delta a$. The minimum distance between the co-elliptic orbit and the reference orbit is always greater than δa.

The crossing condition $(\Delta C_1)^2 = (\Delta C_2)^2 + (\Delta C_3)^2$ is used to determine the relative semi-major axis of the co-elliptic orbit connecting to a particular safe orbit. The differences in C_1, C_2 and C_3 are taken between the co-elliptic orbit and the safe orbit. The crossing condition leads to a second degree polynomial in the relative semi-major axis, meaning that there are two co-elliptic orbits that connect to a particular safe orbit:

$$\eta^4\left(\delta a_{coelliptic}\right)^2 + 2\left\{-(1+e^2)C_{1,safe} + 2eC_{2,safe}\right\}\delta a_{coelliptic} + \left(C_{1,safe}\right)^2 - \left(C_{2,safe}\right)^2 - \left(C_{3,safe}\right)^2 = 0 \tag{66}$$

For a non-drifting safe orbit there is a positive and a negative root. The true anomaly of the intersection is found from Eq. (30). The value of the parameter C_4 is found by equating the x-coordinate at the connection point using Eq. (61) for both possible values of the semi-major axis.

$$\rho_i\eta^2\theta_i^2 C_{4,coelliptic,i} = e(\theta_i^2+2)\sin\vartheta_i\left\{C_{1,safe} - (1+e^2)\delta a_{coelliptic,i}\right\} - 2(\rho_i+e^2)\sin\vartheta_i\left\{C_{2,safe} - 2e\delta a_{coelliptic,i}\right\} + 2\rho_i(e+\cos\vartheta_i)C_{3,safe} + \rho_i\eta^2\theta_i^2 C_{4,safe},\ i=1,2 \quad (67)$$

B. Altering the Drift Rate

Altering the drift rate is performed by means of tangential maneuvers. A two-impulse transfer that lasts one revolution alters the relative mean anomaly without changing any of the other ROE. The first impulse of such a transfer is given by:

$$\Delta V = \frac{an\eta}{6\pi\theta N_{orb}}\Delta M \quad (68)$$

In equation (68) $\Delta M = \delta M_4 - \delta M_2 - 3\pi N_{orb}a^{-1}\delta a_{coelliptic}$, and the term $3\pi\cdot N_{orb}\cdot a^{-1}\cdot\delta a$ represents the drift in the co-elliptic orbit that would have occurred if no maneuvers would have been performed. The second impulse has the same magnitude as the first impulse but opposite in sign.

Equation (68) can be used to set bounds on the number of orbits spent in the drift orbit and determine whether the strategy is feasible for the given initial conditions. The upper bound is found by assuming that the chaser can directly enter the co-elliptic drift orbit and that no ΔV is required to alter the drift rate.

$$N_{orb,\max} = \left\lfloor \frac{\delta M_2 - \delta M_4}{3\pi a^{-1}\delta a_{coelliptic}} \right\rfloor \quad (69)$$

The floor function is used to ensure that an integer number of orbits is spent in the drift orbit. The minimum number of orbits spent in the drift orbit is found by assuming that the ΔV required to initiate the drift is equal in magnitude and opposite in sign to the second ΔV of the cotangential maneuver.

$$N_{orb,\min} = \left\lceil \frac{\delta M_2 - \delta M_4}{3\pi a^{-1}(\delta a_{coelliptic} - 2\theta n^{-1}\eta^{-1}\Delta V_{CTG,2})} \right\rceil \quad (70)$$

The ceiling function is used to ensure that an integer number of orbits is spent in the drift orbit. Note that for the strategy discussed here, $\delta a_{coelliptic} < 0$ and $\Delta V_{CTG,2} > 0$, such that the absolute magnitude of the denominator increases. Equation (69) ensures that the chaser does not move above the co-elliptic orbit, while equation (70) ensures that the chaser does not move below the original orbit. The condition expressed in equation (69) potentially affects the safety of the trajectory, while the condition expressed in equation (70) ensures that the total ΔV required for maneuvers M1, M2 and M4 is equal to the ΔV required for the cotangential maneuver. Equation (70) ensures that the

second impulse of the cotangential maneuver is effectively split to correct the along track distance in the drift orbit. If the condition in equation (70) is violated, then the correcting the along-track distance requires additional ΔV.

Equation (69) establishes a relationship between the altitude of the initial orbit and the along-track distance, and determines whether the rendezvous strategy is feasible given the initial altitude and along-track distance. Equation (69) implies that the difference in mean anomaly at maneuver M2 and maneuver M4 either needs to be equal to zero (in which case M2 and M4 coincide) or greater than or equal to the along-track drift during one orbit to ensure that the chaser can spend at least one orbit in the co-elliptic drift orbit.

C. Drift-Based Rendezvous Strategy Ending in Safe Orbit

The rendezvous strategy shown in Fig. 5 can now be created and simulated. The strategy consists of a cotangential maneuver, a phasing element, and an insertion into a safe orbit. The target state is a (drift-free) safe orbit with alignment. For this safe orbit the elements C_2 and C_3 are computed using Eq. (60), element C_4 using Eq. (62) and C_1 using Eq. (58). The out-of-plane elements C_5 and C_6 are found from Eq. (63). The first step to define the maneuver strategy is to compute a cotangential transfer using Eq. (11), (16) and (18). The cotangential maneuver algorithm provides the true anomaly ϑ_2 at which the second impulse (corresponding to M2 in Fig. 5) needs to be executed and the along-track position C_4 at the end of the transfer. Next, the intersection point of the safe orbit with a co-elliptic drift orbit is obtained from Eq. (66), picking the root that has the same sign as the initial drift orbit. The true anomaly of the intersection is found from Eq. (30). The result is a co-elliptic orbit with elements C_1, C_2 and C_3 found from Eq. (6) and (64) and the along-track element C_4 of the intersection point with the safe orbit given by Eq. (67). The ΔV at the connection point M5 is found by converting the change in C elements to a change in Cartesian state. The difference in the position components are of course equal to zero by definition. The drift orbit is propagated backwards from the true anomaly of the intersection point to the first occurrence of the true anomaly of the second impulse of the cotangential maneuver. This ensures that there are an integer number of orbits between maneuvers M2 and M4. The drift rate between maneuvers M2 and M4 is corrected using tangential maneuvers derived from Eq. (68). The number of orbits spent in the drift orbit is constrained by (1) ensuring that the trajectory remains below a co-elliptic orbit of altitude H1 and (2) that the ΔV at M2 is greater than 0. Condition (1) and (2) together ensure that the total ΔV required for maneuvers M1, M2 and M4 does not exceed the total ΔV for a cotangential maneuver between the initial orbit and the co-elliptic orbit. The final maneuver to be computed is the out-of-plane maneuver M3. The intersection points

with the orbital plane can be found by setting Eq. (52) to zero. The ΔV is then equal in magnitude and opposite in sign to the out-of-plane velocity. All maneuvers are now known.

The strategy is simulated for different values of the eccentricity. Table 1 lists the parameters used for simulation of the approach strategy. The selected safe orbit is drift-free with equal amplitude in the y- and z-directions.

Table 1 Simulation parameters

Parameter	Value
Reference orbit	
Gravitational parameter	398600.61 km^3/s^2
Semi-major axis	13394 km
Eccentricity	0 – 0.5
True anomaly	50°
Initial conditions	
Initial C_4 (along track distance)	-2000 m
Initial co-elliptic orbit altitude H_0	100 m
Safe orbit terminal conditions	
Alignment point	[-80 43.3 -25] m
δa	0 m
Out-of-plane motion ratio λ	1
Phase angle τ_0	0°
True anomaly at alignment	130°

Figure 6 shows the rendezvous strategy for several values of the eccentricity. The number of revolutions spent in the drifting orbit has been set to 2 for all cases. At zero eccentricity the trajectory is very similar to the conceptual sketch shown in Fig. 5. When the eccentricity increases, the trajectory starts to deform more and more with respect to the familiar circular orbit rendezvous trajectory. At the same time, all trajectories successfully intercept the alignment point irrespective of the eccentricity. Figure 6 also shows that as the eccentricity increases, the safe orbit expands outwards. The exact evolution of the shape of the safe orbit with eccentricity is strongly dependent on the details of the geometry (e.g. the true anomaly and the position of the alignment point), meaning that the suitability of the trajectory for a reference orbit of a given eccentricity needs to be examined using the procedures outlined in section IV.B. The same is also true for the co-elliptic drift orbit that connects to the safe orbit.

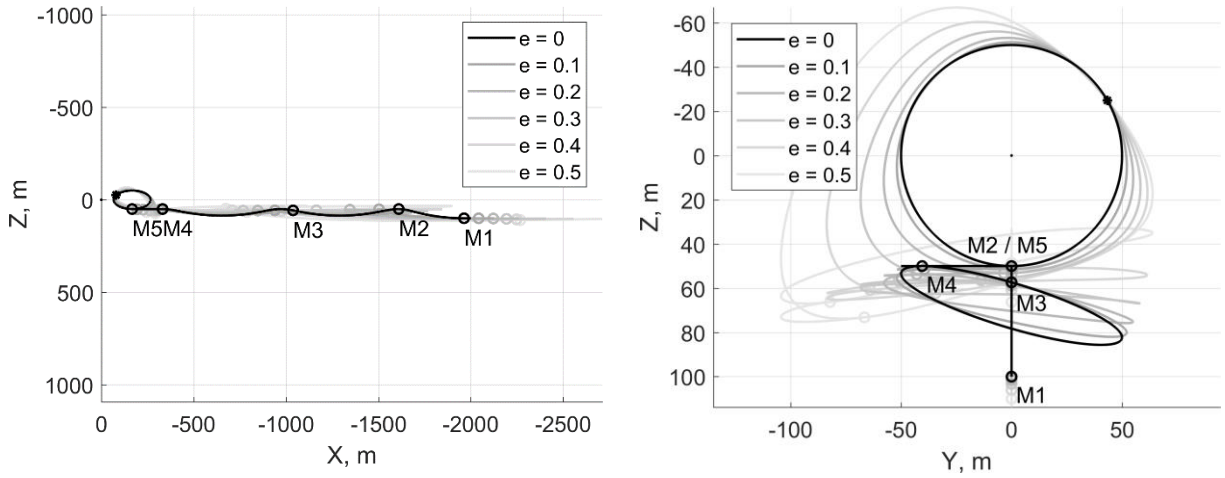

Fig. 6 Simulated rendezvous trajectory in the tangential frame.

Figure 6 shows that at eccentricities of 0.4 and 0.5, the co-elliptic drift orbit that connects to the safe orbit actually enters the circle with radius 50 m centered on the origin in the YZ-projection. This is not necessarily a problem as long as the trajectory does not enter the stay out zone or safety sphere. In this case, if the safety sphere has a radius of 30 m, then the trajectory could still be considered safe. The issue is examined further by examining the calculated parameters of the rendezvous algorithm in Table 2.

Table 2 Calculated parameters for rendezvous strategy

	e = 0	e = 0.1	e = 0.2	e = 0.3	e = 0.4	e = 0.5
C_4 at M2, m	-1609,9	-1604,9	-1593,8	-1575,7	-1548,6	-1508,4
C_4 at M4, m	-331,5	-345,7	-364,4	-388,3	-418,8	-460,3
C_4 at M5, m	-166,6	-175,8	-186,9	-199,5	-213,7	-233,2
δa, (equation (69)), m	-50,0	-51,2	-53,2	-56,0	-59,8	-65,2
δa, (equation (70)), m	-75,0	-75,6	-76,6	-78,0	-79,9	-82,6
$N_{orb,max}$, (equation (69))	2	2	2	2	1	1
$N_{orb,min}$, (equation (70))	2	2	2	2	2	2

Table 2 shows the calculated parameters for the rendezvous strategy for different values of the eccentricity. The first three rows provide the along-track element C_4 for maneuvers M2, M4 and M5. Rows 4 to 7 evaluate the bounds on the number of orbits spent drifting between M2 and M4 that are provided in equations (69) and (70). The maximum number of orbits in the drift orbit is equal to 1 for eccentricities of 0.4 and 0.5, while the minimum number of orbits to be spent in the drift orbit is equal to 2. For all other values of the eccentricity, the minimum and the maximum number of orbits in the drift orbit is equal to 2. Condition (69) is not fulfilled for eccentricities of 0.4 and 0.5, and as a result the drift orbit between maneuver M2 and M4 has its highest point above the co-elliptic drift orbit. In fact, Table 2 shows that for eccentricities of 0.4 and 0.5 either condition (69) or condition (70) needs to be broken. It can be verified that with an initial value of C_4 = 2400 m, the rendezvous can be completed at eccentricities of 0.4 and 0.5

while fulfilling condition (69), but that the lower eccentricity cases would need 3 orbits for completing the drift. For the sake of maintaining the number of drift orbits the same across all values of the eccentricity, the non-fulfilment of condition (69) is deemed acceptable in this example, because maintaining the number of drift orbits facilitates the visual comparison of the trajectories and also illustrates the consequences of non-fulfilment of these conditions.

The algorithms work for any arbitrary eccentricity; however, Fig. 6 and 7 show that the rendezvous trajectory progressively deviates from the familiar circular rendezvous trajectory as the eccentricity increases. The reason for this is that the scaling factors ρ and θ depend on the eccentricity. Note that the scaling factors also depend on the true anomaly. This causes the geometry of particular rendezvous trajectories to be dependent on the true anomaly of key points of the trajectory such as the alignment point and the starting point. It also means that the geometry of the trajectory is not fully known a priori, especially for high-eccentricity orbit rendezvous. From a practical point of view this means that for high-eccentricity orbit rendezvous the safety and feasibility of the rendezvous trajectory needs to be analyzed during the mission design. During mission design, trajectory design parameters such as the altitude of drift orbits and the dimensions of safe orbits need to be adjusted according to a trajectory safety and feasibility analysis.

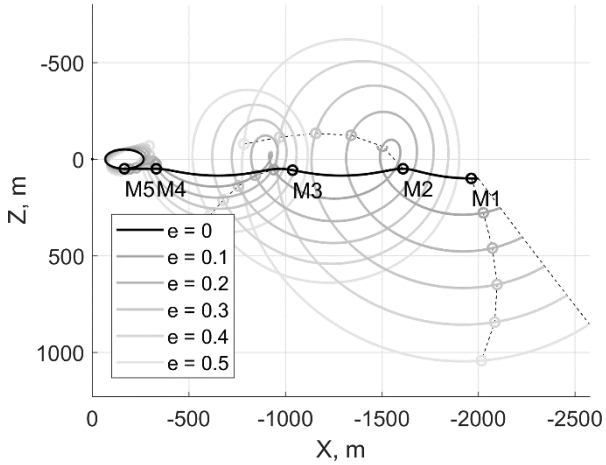

Fig. 7 Simulated rendezvous trajectory in the LVLH frame.

Figure 7 shows the same set of rendezvous trajectories in the LVLH frame. In Fig. 7 the locus of the locations of the maneuvers as they evolve with increasing eccentricity is indicated by means of a dotted line. Figure 7 shows that it is not obvious how to generate such a trajectory given only Cartesian coordinates in the LVLH frame. Trajectory safety of rendezvous trajectories in elliptic orbit rendezvous cannot be established as easily by inspecting the trajectory in the LVLH frame as it is in the tangential frame of Fig. 6, because the z-coordinate shows a much greater variation.

Of course the trajectory for zero eccentricity in the LVLH frame corresponds exactly to the trajectory for zero eccentricity in the tangential frame.

Table 3 shows the maneuver times for the rendezvous strategy expressed as multiples of the orbital period. Table 3 shows that the time at which the in-plane maneuvers M1, M2, M4 and M5 occur remains fairly constant over the different values of the eccentricity. The out-of-plane maneuver M3 occurs almost half an hour earlier in the case of e = 0.5 with respect to the circular orbit.

Table 3 Maneuver times for rendezvous strategy

	e = 0	e = 0.1	e = 0.2	e = 0.3	e = 0.4	e = 0.5
man. no.	time, h	time, h	time, h	time, h	time, h	time, h
M1	0.167	0.167	0.167	0.167	0.167	0.167
M2	2.309	2.309	2.306	2.301	2.294	2.286
M3	5.952	5.954	5.901	5.800	5.664	5.501
M4	10.880	10.879	10.877	10.872	10.865	10.857
M5	12.380	12.379	12.363	12.335	12.294	12.230

Table 4 shows the ΔV required to perform this rendezvous strategy for various values of the eccentricity. Only the magnitude of the ΔV is given. The in-plane maneuvers M1, M2, M4 and M5 are performed in the direction of the local orbital velocity vector, and the out-of-plane maneuver M3 is performed in the out-of-plane direction. The second ΔV of the cotangential maneuver is modified to alter the drift rate, and the sum of the ΔV's required for maneuvers M1, M2 and M4 (the sequence of orbit raising and drift correcting maneuvers) is equal to the ΔV required for a cotangential maneuver from the original orbit to the co-elliptic orbit. The cases for which the eccentricity is 0.4 and 0.5 do not fulfil condition (69). As a consequence, additional ΔV is spent to correct the in-plane element C_4. The ΔV for the cotangential maneuver alone is given in brackets for these cases. The total ΔV required for M1, M2 and M4 can be compared to the ΔV lower bound [24] given by equation (19). The dominant change is the change in relative semi-major axis. As in the work of Chernick and D'Amico [24], the out-of-plane maneuver M3 is performed at the relative node and therefore optimally changes the out-of-plane motion. Maneuver M5 is performed at the intersection of the safe orbit with the co-elliptic orbit by design.

Table 4 ΔV required for rendezvous strategy

	e = 0	e = 0.1	e = 0.2	e = 0.3	e = 0.4	e = 0.5
man. no.	ΔV, mm/s	ΔV, mm/s	ΔV, mm/s	ΔV, mm/s	ΔV, mm/s	ΔV, mm/s
M1	5.09	4.73	4.28	3.77	3.21	2.59
M2	1.46	1.99	3.02	4.73	7.45	11.73
M3	20.36	19.26	19.18	20.04	21.77	24.31
M4	3.63	3.30	2.54	1.09	1.45	5.80
M5	10.18	9.44	8.87	8.59	8.92	10.46

M1+M2+M4	10.18	10.01	9.84	9.60	12.11 (9.21)	20.12 (8.53)
Lower bound	10.18	8.98	7.78	6.58	5.36	4.10
Total	40.73	38.71	37.89	38.23	42.80 (39.90)	54.89 (43.30)

Table 4 shows that there is considerable variation in the ΔV associated with each of the maneuvers depending on the eccentricity of the reference orbit. The order of magnitude of maneuvers is similar for most maneuvers apart from the second maneuver, which grows from 1.46 mm/s to 11.73 mm/s as the eccentricity grows from 0 to 0.5. The evolution of the ΔV for each of the maneuvers strongly depends on the local geometry of the trajectory at the time of the maneuver, and there is no particular pattern in the dependency on the eccentricity of the reference orbit. It should be noted that the sequence of maneuvers generated here is quite artificial; as Fig. 7 shows the initial conditions have been idealized over the different values of the eccentricity in order to facilitate easy visual comparison of the trajectories and to demonstrate the general applicability of the trajectory and maneuver definition strategy. It should be stressed that this selection of the initial conditions is purely for this reason. The strategy is applicable in general for different initial values of the true anomaly and variation in the initial conditions, as long as sufficient along-track distance (as established by equations (69) and (70)) is available to perform the strategy. More explicitly, for a given safe orbit, the procedure to check the along-track distance is as follows. First, equation (11) provides the transfer angle of the cotangential transfer and with that the true anomaly ϑ_2 of maneuver M2. Equation (18) provides C_4 at the end of the cotangential transfer. Equation (30) and (67) provide the true anomaly and C_4 at the maneuver M5. Back-propagation of the co-elliptic drift orbit from maneuver M5 to the first occurrence of ϑ_2 before maneuver M5 leads to C_4 of maneuver M4. The values of C_4 need to be converted to relative mean anomaly, and equation (66) needs to be used to find the relative semi-major axis of the co-elliptic orbit. Now, equation (69) can be used to establish whether sufficient along-track distance is available to perform the strategy.

VI. Conclusion

This paper has created a clear connection between the traditional strategies for rendezvous in circular orbits and corresponding strategies in elliptical orbits. The cotangential transfer for elliptic orbit rendezvous is conceptually similar to the Hohmann transfer in circular orbit rendezvous. In both cases, the ΔV is applied in the direction of the local orbital velocity vector and the z-coordinate or its equivalent in an elliptic reference orbit responds with a change of mean altitude and amplitude of the motion. Some differences do exist. For the linear Hohmann transfer in circular orbit rendezvous, the first and the second ΔV are exactly equal, while in elliptic orbit rendezvous the two ΔV's are

generally different in magnitude. The solution of the cotangential transfer leads to a natural definition of a new set of relative orbital elements. The representation of the trajectory in terms of these elements creates a connection to the travelling ellipse formulation in circular orbits, and this concept can aid in the development and analysis of rendezvous strategies. This representation also facilitates the determination of whether two trajectories intersect. Finally, the new set of relative orbital elements can be used to define safe trajectories with and without drift. These safe orbits represent a generalization to non-circular orbits of the safe orbits based on eccentricity / inclination vector separation that are used in circular orbit rendezvous and formation flying.

The combination of the cotangential transfers and safe orbits leads to a useful conceptual approach to defining rendezvous trajectories for elliptical orbits. An analysis of a drift-based rendezvous strategy shows that the same strategy can be applied for both circular and eccentric reference orbits with similar results in terms of maneuver application times and ΔV magnitudes. In this sense, classical rendezvous strategies developed for circular orbit rendezvous can be fully generalized following the procedures outlined in this paper.

Acknowledgement

This work is the result of several years of development, partly performed at GMV with internal funds and partly performed in the frame of different European Space Agency (ESA) funded activities/applications, including HARVD (ESA contract No. 4200019846), iGNC (ESA contract No. 4000103644/11/NL/EK) and AnDROiD (ESA contract 4000110200/14/NL/MV).

Appendix A: Details of TAN frame

The transformation matrix $\mathbf{T}_\gamma$ takes a vector from the TAN frame to the LVLH frame, that is to say:

$$\mathbf{x}_{LVLH} = \mathbf{T}_\gamma \mathbf{x}_{TAN} \tag{71}$$

The matrix $\mathbf{T}_\gamma$ and its inverse are composed of a rotation matrix and an angular velocity matrix.

$$\mathbf{T}_\gamma = \begin{bmatrix} \mathbf{R}_\gamma & \mathbf{0} \\ -\boldsymbol{\Omega}_\gamma \mathbf{R}_\gamma & \mathbf{R}_\gamma \end{bmatrix}, \ \mathbf{T}_\gamma^{-1} = \begin{bmatrix} \mathbf{R}_\gamma^T & \mathbf{0} \\ \mathbf{R}_\gamma^T \boldsymbol{\Omega}_\gamma & \mathbf{R}_\gamma^T \end{bmatrix} \tag{72}$$

The rotation matrix for the flight-path angle is given by:

$$\mathbf{R}_\gamma = \begin{bmatrix} \cos\gamma & \sin\gamma \\ -\sin\gamma & \cos\gamma \end{bmatrix} = \theta^{-1} \begin{bmatrix} \rho & e\sin\vartheta \\ -e\sin\vartheta & \rho \end{bmatrix} \tag{73}$$

The angular velocity matrix is given by:

$$\boldsymbol{\Omega}_{\gamma} = \begin{bmatrix} 0 & -\dot{\gamma} \\ \dot{\gamma} & 0 \end{bmatrix} = \eta^{-3} n \rho^2 \theta^{-2} (\rho - \eta^2) \begin{bmatrix} 0 & -1 \\ 1 & 0 \end{bmatrix} \tag{74}$$

Appendix B: Details of element set C

This appendix summarizes the relationships between the C elements, the relative Kepler elements, the Yanamaka-Ankersen integration constants and the state vector in the tangential frame. Linear transformations between different sets of ROE can be represented as matrices of partial derivatives. The transformation from Kepler elements to C elements is given by the matrix of partials from the C elements to the Kepler orbital elements.

$$\frac{\partial \mathbf{c}}{\partial \mathbf{k}} = p \begin{bmatrix} a^{-1} & -2e\eta^{-2} & 0 & 0 & 0 & 0 \\ ea^{-1} & -(1+e^2)\eta^{-2} & 0 & 0 & 0 & 0 \\ 0 & 0 & 0 & -e\cos i & -e & 0 \\ 0 & 0 & 0 & \eta^{-2}\cos i & \eta^{-2} & \eta^{-3} \\ 0 & 0 & -\cos\omega & -\sin i \sin\omega & 0 & 0 \\ 0 & 0 & \sin\omega & -\sin i \cos\omega & 0 & 0 \end{bmatrix} \tag{75}$$

The matrix of partials from the Kepler orbital elements to the C elements is given by:

$$\frac{\partial \mathbf{k}}{\partial \mathbf{c}} = \frac{1}{p} \begin{bmatrix} a\eta^{-2}(1+e^2) & -2ae\eta^{-2} & 0 & 0 & 0 & 0 \\ e & -1 & 0 & 0 & 0 & 0 \\ 0 & 0 & 0 & 0 & -\cos\omega & \sin\omega \\ 0 & 0 & 0 & 0 & -\frac{\sin\omega}{\sin i} & -\frac{\cos\omega}{\sin i} \\ 0 & 0 & -e^{-1} & 0 & \cot i \sin\omega & \cot i \cos\omega \\ 0 & 0 & e^{-1}\eta & \eta^3 & 0 & 0 \end{bmatrix} \tag{76}$$

The elements C can also be related to the Yamanaka-Ankersen set of trajectory integration constants [26]. The order of the integration constants is the same as in the original paper by Yamanaka and Ankersen. The linear transformation matrix from the Yamanaka-Ankersen integration constant to the elements C is given by:

$$\frac{\partial \mathbf{c}}{\partial \mathbf{y}} = \begin{bmatrix} 0 & 0 & -2e & -2 & 0 & 0 \\ 0 & 0 & -(1+e^2) & -2e & 0 & 0 \\ -e & -1 & 0 & 0 & 0 & 0 \\ \eta^{-2} & e\eta^{-2} & 0 & 0 & 0 & 0 \\ 0 & 0 & 0 & 0 & 0 & 1 \\ 0 & 0 & 0 & 0 & -1 & 0 \end{bmatrix} \tag{77}$$

The linear transformation matrix from the elements C to the Yamanaka-Ankersen integration constant is given by:

$$\frac{\partial \mathbf{y}}{\partial \mathbf{C}} = \begin{bmatrix} 0 & 0 & e\eta^{-2} & 1 & 0 & 0 \\ 0 & 0 & -\eta^{-2} & -e & 0 & 0 \\ e\eta^{-2} & -\eta^{-2} & 0 & 0 & 0 & 0 \\ -\frac{1}{2}(1+e^2)\eta^{-2} & e\eta^{-2} & 0 & 0 & 0 & 0 \\ 0 & 0 & 0 & 0 & 0 & -1 \\ 0 & 0 & 0 & 0 & 1 & 0 \end{bmatrix} \tag{78}$$

The Yamanaka-Ankersen equations are non-singular if the eccentricity goes to zero [26]. Equations (77) and (78) do not contain any divisors of the eccentricity, indicating that the transformation from the C elements and the Yamanaka-Ankersen set of trajectory integration constants is non-singular if the eccentricity goes to zero.

To obtain the linear mapping matrix from the C element vector to the Cartesian state in the TAN frame, the following expression needs to be evaluated:

$$\mathbf{B}_{C,TAN} = \mathbf{T}_{\gamma}^{-1}\mathbf{B}\frac{\partial \mathbf{C}}{\partial \mathbf{k}} \tag{79}$$

The elements of the linear mapping matrix from the C element vector to the Cartesian state in the TAN frame can then be found as:

$$\begin{aligned}
&\mathbf{B}_{C,TAN}(1,1) = \rho^{-1}\eta^{-2}\theta^{-1}\{e(\theta^2+2)\sin\vartheta\}, && \mathbf{B}_{C,TAN}(2,1) = -\rho^{-1}\theta^{-1}, \\
&\mathbf{B}_{C,TAN}(1,2) = \rho^{-1}\eta^{-2}\theta^{-1}\{-2(\rho+e^2)\sin\vartheta\}, && \mathbf{B}_{C,TAN}(2,2) = -\rho^{-1}\theta^{-1}\cos\vartheta\,, \\
&\mathbf{B}_{C,TAN}(1,3) = \rho^{-1}\eta^{-2}\theta^{-1}\{2(e+cos\,\vartheta)\rho\}, && \mathbf{B}_{C,TAN}(2,3) = -\rho^{-1}\theta^{-1}\sin\vartheta\,, \\
&\mathbf{B}_{C,TAN}(1,4) = \theta, && \mathbf{B}_{C,TAN}(2,4) = 0, \\
&\mathbf{B}_{C,TAN}(3,1) = n\eta^{-5}\theta^{-3}\left\{\tfrac{1}{2}(1+e^2)\theta^2 + \rho^3(\theta^2-2)\right\}, \\
&\mathbf{B}_{C,TAN}(3,2) = n\eta^{-5}\theta^{-3}\{(4e^2[e^2+\rho]-2\rho^3)\cos\vartheta + e(1+e^2)\}, \\
&\mathbf{B}_{C,TAN}(3,3) = n\eta^{-5}\theta^{-3}\{-2\rho^3\sin\vartheta\}, \\
&\mathbf{B}_{C,TAN}(3,4) = n\eta^{-3}\theta^{-1}\{-\rho^2 e\sin\vartheta\}, \\
&\mathbf{B}_{C,TAN}(4,1) = n\eta^{-3}\theta^{-3}\{-(\theta^2+\rho)e\sin\vartheta\}, \\
&\mathbf{B}_{C,TAN}(4,2) = n\eta^{-3}\theta^{-3}\{(\theta^2+\rho[1-\rho])\sin\vartheta\}, \\
&\mathbf{B}_{C,TAN}(4,3) = n\eta^{-3}\theta^{-3}\{(4\eta^2+\rho^2-3[\rho+1])\cos\vartheta - e(2+e^2)\}, \\
&\mathbf{B}_{C,TAN}(4,4) = 0
\end{aligned} \tag{80}$$

Similarly, the inverse mapping can be found from:

$$\mathbf{B}_{C,TAN}^{-1} = \left(\frac{\partial \mathbf{C}}{\partial \mathbf{k}}\right)^{-1}\mathbf{B}^{-1}\mathbf{T}_{\gamma} \tag{81}$$

The elements of the linear mapping matrix from the Cartesian state in the TAN frame to the C element vector can then be found as:

$$
\begin{aligned}
&\mathbf{B}_{C,TAN}^{-1}(1,1) = \theta^{-3}\{2e\rho^2 \sin\vartheta\},\\
&\mathbf{B}_{C,TAN}^{-1}(2,1) = \theta^{-3}\{-2e\rho^2 \sin\vartheta\cos\vartheta\},\\
&\mathbf{B}_{C,TAN}^{-1}(3,1) = \theta^{-3}\{-2e\rho^2 \sin^2\vartheta\},\\
&\mathbf{B}_{C,TAN}^{-1}(4,1) = \eta^{-2}\theta^{-3}\{2\rho^3 - \theta^2\},\\
&\mathbf{B}_{C,TAN}^{-1}(1,2) = \theta^{-3}\{-2(\rho^3 + \theta^2)\},\\
&\mathbf{B}_{C,TAN}^{-1}(2,2) = \theta^{-3}\begin{Bmatrix}[4\rho^3 + (1+e^2)\rho^2 - 3(1+e^2)\rho - 4(1+e^2)^2 + 5(1+e^2)]\cos\vartheta\\ -e(1+e^2)(2+e^2)\end{Bmatrix},\\
&\mathbf{B}_{C,TAN}^{-1}(3,2) = \theta^{-3}\{\theta^2 + \rho(\eta^2 + \rho[\theta^2 + 2e\cos\vartheta])\}\sin\vartheta\,,\\
&\mathbf{B}_{C,TAN}^{-1}(4,2) = \eta^{-2}\theta^{-3}\{2e\rho^2 \sin\vartheta\},\\
&\mathbf{B}_{C,TAN}^{-1}(1,3) = n^{-1}\eta^3\theta^{-1}\{2\},\\
&\mathbf{B}_{C,TAN}^{-1}(2,3) = n^{-1}\eta^3\theta^{-1}\{-2\cos\vartheta\},\\
&\mathbf{B}_{C,TAN}^{-1}(3,3) = n^{-1}\eta^3\theta^{-1}\{-2\sin\vartheta\},\\
&\mathbf{B}_{C,TAN}^{-1}(4,3) = n^{-1}\eta\rho^{-1}\theta^{-1}\{-2e\sin\vartheta\},\\
&\mathbf{B}_{C,TAN}^{-1}(1,4) = n^{-1}\eta^3\rho^{-1}\theta^{-1}\{2e\sin\vartheta\},\\
&\mathbf{B}_{C,TAN}^{-1}(2,4) = n^{-1}\eta^3\rho^{-1}\theta^{-1}\{(1+e^2)\sin\vartheta\},\\
&\mathbf{B}_{C,TAN}^{-1}(3,4) = n^{-1}\eta^3\rho^{-1}\theta^{-1}\{-[(1+e^2)\cos\vartheta + 2e]\},\\
&\mathbf{B}_{C,TAN}^{-1}(4,4) = n^{-1}\eta\theta^{-1}\{2\},
\end{aligned}
\tag{82}
$$

Neither the linear mapping matrix from the C element vector to the Cartesian state in the TAN frame nor its inverse contains the eccentricity as a divisor. This implies that the C elements do not become singular when the eccentricity goes to zero. In fact, if the eccentricity approaches zero, the expressions in the matrices $\mathbf{B}_{C,TAN}$ and $\mathbf{B}_{C,TAN}^{-1}$ can be compared to the travelling ellipse formulation used in circular orbit rendezvous [55]. If the eccentricity approaches zero, the matrix $\mathbf{B}_{\mathrm{C,TAN}}$ becomes:

$$
\lim_{e\downarrow 0}\mathbf{B}_{C,TAN} = \begin{bmatrix} 0 & -2\sin\vartheta & 2\cos\vartheta & 1\\ -1 & -\cos\vartheta & -\sin\vartheta & 0\\ -\frac{3}{2}n & -2n\cos\vartheta & -2n\sin\vartheta & 0\\ 0 & n\sin\vartheta & -n\cos\vartheta & 0 \end{bmatrix} \tag{83}
$$

And the matrix $\mathbf{B}^{-1}{}_{\mathrm{C,TAN}}$:

$$
\lim_{e\downarrow 0}\mathbf{B}_{C,TAN}^{-1} = \begin{bmatrix} 0 & -4 & 2n^{-1} & 0\\ 0 & 3\cos\vartheta & -2n^{-1}\cos\vartheta & n^{-1}\sin\vartheta\\ 0 & 3\sin\vartheta & -2n^{-1}\sin\vartheta & -n^{-1}\cos\vartheta\\ 1 & 0 & 0 & 2n^{-1} \end{bmatrix} \tag{84}
$$

The parameter C_1 represents the altitude of the center of the ellipse, the parameter C_4 represents the along-track distance of the center of the ellipse and the parameters C_2 and C_3 parameterize the 2 x 1 travelling ellipse.

For completeness, the ROE transition matrix for the C elements is given by:

$$\boldsymbol{\Phi}_C = \frac{\partial \mathbf{C}}{\partial \boldsymbol{\delta\alpha}} \boldsymbol{\Phi}_\alpha \left(\frac{\partial \mathbf{C}}{\partial \boldsymbol{\delta\alpha}}\right)^{-1} = \begin{bmatrix} 1 & 0 & 0 & 0 \\ 0 & 1 & 0 & 0 \\ 0 & 0 & 1 & 0 \\ -\frac{3}{2}\eta^{-5}(1+e^2)n\,t & -3e\eta^{-5}nt & 0 & 1 \end{bmatrix} \tag{85}$$

References

[1] Woffinden, D. C., Geller, D. K., 2009, "Observability Criteria for Angles-Only Navigation," IEEE Transactions on Aerospace and Electronic Systems, Vol. 45, Iss. 3, pp. 1194 - 1208, DOI: 10.1109/TAES.2009.5259193

[2] Woffinden, D. C., Geller, D. K., 2007, "Relative Angles-Only Navigation and Pose Estimation For Autonomous Orbital Rendezvous," Journal of Guidance, Control, and Dynamics, Vol. 30, No. 5 (2007), pp. 1455-1469., DOI: 10.2514/1.28216

[3] Gaias, G., D'Amico, S., Ardaens, J.-S., 2014, "Angles-Only Navigation to a Noncooperative Satellite Using Relative Orbital Elements", Journal of Guidance, Control, and Dynamics, Vol. 37, No. 2 (2014), pp. 439-451., DOI: 10.2514/1.61494

[4] Lovell, T. A, T. Lee, T., 2014, "Nonlinear Observability for Relative Satellite Orbits with Angles-Only Measurements," Proceedings of the International Symposium on Space Flight Dynamics

[5] Sullivan J., Koenig A., D'Amico S., 2016, "Improved Maneuver-Free Approach to Angles-Only Navigation for Space Rendezvous," Proceedings of the 26th AAS/AIAA Space Flight Mechanics Meeting, Napa, CA, February 14-18, 2016.

[6] Montenbruck, O., Gill, E., "Introductory Astrodynamics," Satellite Orbits – Models, Methods, and Applications, Springer-Verlag, Berlin Heidelberg, 2000, pp. 15 – 51, DOI: 10.1007/978-3-642-58351-3

[7] Bate, R. R., Mueller, D. D., White, J. E., 1971, "Orbit Determination From Observation," Fundamentals of Astrodynamics, Dover Publications, 1971, pp. 51 – 150

[8] Legendre, P., Deguine, B., Garmier, R., Revelin, B., 2006, "Two Line Element Accuracy Assessment Based On A Mixture of Gaussian Laws", Proceedings of the AIAA/AAS Astrodynamics Specialist Conference and Exhibit, Guidance, Navigation, and Control and Co-located Conferences, DOI: 10.2514/6.2006-6518

[9] D'Amico S., Ardaens J., Gaias G., Benninghoff H., Schlepp B., Joergensen J. L., 2013, "Noncooperative Rendezvous using Angles-only Optical Navigation: System Design and Flight Results," Journal of Guidance, Control, and Dynamics, Vol. 36, No. 6, (2013) pp. 1576-1595, DOI: 10.2514/1.59236

[10] Peters, T. V., Escorial Olmos, D., 2014, "Relative mission analysis for PROBA-3: safe orbits and CAM," Int. J. of Space Science and Engineering, 2014 Vol.2, No.2, pp.135 – 156. DOI: 10.1504/IJSPACESE.2014.060599

[11] D'Amico, S., Montenbruck, O., "Proximity Operations of Formation-Flying Spacecraft Using an Eccentricity / Inclination Vector Separation," AIAA Journal of Guidance, Control, and Dynamics, Vol. 29, No. 3, 2006, pp. 554–563. DOI: 10.2514/1.15114

[12] Fehse W., "Orbit Dynamics and Trajectory Elements," *Automated Rendezvous and Docking of Spacecraft*, 1st ed., Cambridge University Press, Cambridge (UK), 2003, pp. 29-75, DOI: 10.1017/CBO9780511543388

[13] Gabriella Gaias and Jean-Sébastien Ardaens. "Flight Demonstration of Autonomous Noncooperative Rendezvous in Low Earth Orbit", Journal of Guidance, Control, and Dynamics, Vol. 41, No. 6 (2018), pp. 1337-1354. DOI: 10.2514/1.G003239

[14] Wen, W. L.-S., 1961, "A Study of Cotangential, Elliptical Transfer Orbits in Space Flight", Journal of the Aerospace Sciences, Vol. 28, No. 5 (1961), pp. 411-417., DOI: 10.2514/8.9010

[15] Zhang, G., Zhou, Di, Mortari, D., Henderson, T. A., "Analytical Study of Tangent Orbit and Conditions for Its Solution Existence", *AIAA Journal of Guidance, Control, and Dynamics*, Vol. 35, No. 1, January–February 2012, pp. 186-194 DOI: 10.2514/1.53396

[16] Doll, J. R., Gobetz, F. W., "A survey of impulsive trajectories," *AIAA Journal*, Vol. 7, No. 5, 1969, pp. 801-834. DOI: 10.2514/3.5231

[17] Moyer, H. G., "An analytic treatment of cotangential transfer," *AIAA Journal*, Vol. 5, No. 6, 1967, pp. 1197-1198. DOI: 10.2514/3.4164

[18] Bender, D. F., "Optimum coplanar two-impulse transfers between elliptic orbits," Aerospace Engineering, pp. 44–52, 1962

[19] Burns, R. E., 1989, "Forbidden tangential orbit transfers between intersecting Keplerian orbits," Acta Astronautica, Vol. 19, No. 8, pp. 649–656, DOI: 10.1016/0094-5765(89)90133-1

[20] Zhang, G., Wang, D., Cao, X., Sun, Z., 2013, "Tangent Orbital Rendezvous Using Linear Relative Motion with J2 Perturbations," Mathematical Problems in Engineering, vol. 2013, Article ID 531672, 8 pages, 2013. DOI: 10.1155/2013/531672

[21] Peters, T. V., Strippoli, L., "Innovative Guidance Techniques for Rendezvous on Elliptic Orbits," Proceedings of the 4th International Conference on Astrodynamics Tools and Techniques, 3 - 6 May 2010.

[22] Yin J., Han C., 2013, "Elliptical formation control based on relative orbit elements," Chinese Journal of Aeronautics, Vol. 26, No.6, (2013), pp. 1554–1567, DOI: 10.1016/j.cja.2013.07.014

[23] Gaias, G., D'Amico, S., 2015, "Impulsive Maneuvers for Formation Reconfiguration Using ROE," Journal of Guidance, Control, and Dynamics, Vol.38, No.6, 2015, pp. 1036-1049, DOI: 10.2514/1.G000189

[24] Chernick, M., D'Amico, S., 2018, "New Closed-Form Solutions for Optimal Impulsive Control of Spacecraft Relative Motion", Journal of Guidance, Control, and Dynamics, Vol.41, No.2, 2018, pp. 301-319, DOI: 10.2514/1.G002848

[25] Chernick M., D'Amico S., 2018, "Closed-Form Optimal Impulsive Control of Spacecraft Formations using Reachable Set Theory," 2018 AAS/AIAA Astrodynamics Specialist Conference, Snowbird, UT, August 19-23 (2018)

[26] Yamanaka, K., Ankersen, F., "New State Transition Matrix for Relative Motion on an Arbitrary Elliptical Orbit," AIAA Journal of Guidance, Control and Dynamics, Vol. 25, No. 1, Jan.-Feb. 2002, pp. 60-66, DOI: 10.2514/2.4875

[27] Montenbruck, O., Gill, E., "Linearization," Satellite Orbits – Models, Methods, and Applications, Springer-Verlag, Berlin Heidelberg, 2000, pp. 233-256, DOI: 10.1007/978-3-642-58351-3

[28] Schaub, H., Junkins, J.L., “Spacecraft Formation Flying,” Analytical Mechanics of Space Systems, AIAA, Reston VA, 2003, pp. 593-674, DOI: 10.2514/4.861550

[29] Sullivan J., D’Amico S., 2017, ”Nonlinear Kalman Filtering for Improved Angles-Only Navigation Using ROE,” Journal of Guidance, Control, and Dynamics, Vol. 40, No. 9, pp. 2183-2200, DOI: 10.2514/1.G002719

[30] Clohessy, W. H., and Wiltshire, R. S., “Terminal Guidance System for Satellite Rendezvous,” Journal of Aerospace Sciences, Vol. 27, 1960, pp. 653-658, DOI: 10.2514/8.8704

[31] D’Amico, S., “Relative Orbital Elements as Integration Constants of the Hill’s Equations,” DLR TN 05-08, Oberpfaffenhofen, Dec. 2005

[32] Arsenault, J. L., Ford, K. C., Koskela, P. E., “Orbit Determination Using Analytic Partial Derivatives of Perturbed Motion,” AIAA Journal, Vol. 8, No. 1, Jan. 1970, pp. 4-12 DOI: 10.2514/3.5597

[33] Gim D.-W., Alfriend K. T., “State Transition Matrix of Relative Motion for the Perturbed Noncircular Reference Orbit,” AIAA Journal of Guidance, Control and Dynamics, Vol. 26, No. 6, Nov-Dec 2003, pp. 956-971, DOI: 10.2514/2.6924

[34] Alfriend, K.T., Vadali, S.R., Gurfil, P., How, J.P., Breger, L. “Linear equations of relative motion,” Spacecraft formation flying: dynamics, control and navigation, Elsevier, Oxford, 2010, pp. 83-121 DOI: 10.2514/5.9781600861550.0593.0673

[35] Lara, M., and Gurfil, P., “Integrable Approximation of J2-Perturbed Relative Orbits,” Celestial Mechanics and Dynamical Astronomy, Vol. 114, No. 3, 2012, pp. 229–254., DOI: 10.1007/s10569-012-9437-8

[36] Ben-Yaacov, O., Gurfil, P., 2013, "Long-term cluster flight of multiple satellites using differential drag," Journal of Guidance Control Dynamics, Vol. 36, No. 6, (2013), pp. 1731–1740, DOI: 10.2514/1.61496

[37] Gaias, G., Ardaens, J. S., Montenbruck, O., “Model of J2 Perturbed Satellite Relative Motion with Time-Varying Differential Drag,” Celestial Mechanics and Dynamical Astronomy, Vol. 123, No. 4, 2015, pp. 411–433., DOI: 10.1007/s10569-015-9643-2

[38] Koenig A.W., Guffanti T., D'Amico S., 2017, “New State Transition Matrices for Spacecraft Relative Motion in Perturbed Orbits,” Journal of Guidance, Control, and Dynamics, Vol. 40, No. 7, pp. 1749-1768 (September 2017) DOI: 10.2514/1.G002409

[39] Fehse W., “Approach Safety and Collision Avoidance,” *Automated Rendezvous and Docking of Spacecraft*, 1st ed., Cambridge University Press, Cambridge (UK), 2003, pp. 76-107, DOI: 10.1017/CBO9780511543388

[40] Peters, T.V., Noomen, R., Colmenarejo, P., 2014, “Analytical Solutions to Two-Impulse Nondrifting Transfer Problems for Rendezvous in Elliptical Orbits,” Journal of Guidance, Control, and Dynamics, Vol. 37, No. 3 (2014), pp. 775-788. DOI: 10.2514/1.61885

[41] Peters, T. V., Strippoli, L., “Guidance for Elliptic Orbit Rendezvous,” AAS 10-175, *Proceedings of the 20th AAS/AIAA Spaceflight Mechanics Meeting*, 14-17 February 2010, San Diego, CA

[42] Battin, R.H., 1999, "Variation of Parameters," An Introduction to the Mathematics and Methods of Astrodynamics, AIAA (1999), pp. 471-514, ISBN: 0-930403-25-8, DOI: 10.2514/4.861543

[43] Riggi L., D'Amico S., 2016, "Optimal Impulsive Closed-Form Control for Spacecraft Formation Flying and Rendezvous," Proceedings of the 2016 American Control Conference, July 6–8, Boston, MA, USA, DOI: 10.1109/ACC.2016.7526587

[44] Zhang, G., Zhou, D., Sun, Z., and Cao, X., 2013, "Optimal Two-Impulse Cotangent Rendezvous Between Coplanar Elliptical Orbits", Journal of Guidance, Control, and Dynamics, Vol. 36, No. 3 (2013), pp. 677-685. DOI: 10.2514/1.59191

[45] Battin, R.H., 1999, "Two-Body Orbital Boundary-Value Problem," An Introduction to the Mathematics and Methods of Astrodynamics, AIAA (1999), pp. 237-294, ISBN: 0-930403-25-8, DOI: 10.2514/4.861543

[46] Strippoli, L., Novelli, G., Gil Fernandez, J., Colmenarejo, P., Le Peuvedic, C., Lanza, P., Ankersen, F., 2015, "Integrated vision-based GNC for autonomous rendezvous and capture around Mars," CEAS Space Journal 7, pp. 143-157, DOI: 10.1007/s12567-015-0090-4

[47] Chao, C.-C., 2005, "Advanced Concepts of Orbit Control," Applied Orbit Perturbation and Maintenance, The Aerospace Press, AIAA, ISBN: 978-1-884989-17-9, DOI: 10.2514/4.989179

[48] De Florio, S., D'Amico, S., Radice, G., 2013, "Flight Results of Precise Autonomous Orbit Keeping Experiment on PRISMA Mission," Journal of Spacecraft and Rockets, Vol. 50, No. 3, pp. 662-674, DOI: 10.2514/1.A32347

[49] Montenbruck, O., Kirschner, M., D'Amico, S., Bettadpur S., 2006, "E/I-Vector Separation for Safe Switching of the GRACE Formation," Aerospace Science and Technology, Vol. 10, No. 7, pp. 628-635 (2006), DOI: 10.1016/j.ast.2006.04.001

[50] Montenbruck, O., Kahle, R., D'Amico, S., Ardaens, J.-S., 2008, "Navigation and Control of the TanDEM-X Formation," Journal of the Astronautical Sciences, Vol. 56, No. 3, pp. 341-357, DOI: 10.1007/BF03256557

[51] Jiang, F., Li, J., Baoyin, H., Gao, Y., 2008, "Study on Relative Orbit Geometry of Spacecraft Formations in Elliptical Reference Orbits," AIAA Journal of Guidance, Control, and Dynamics, Vol. 31, No. 1, January–February 2008, pp. 123-134, DOI: 10.2514/1.30394

[52] Dang, Zh., Wang, Zh., Zhang, Y., 2014, "Modeling and Analysis of the Bounds of Periodical Satellite Relative Motion", Journal of Guidance, Control, and Dynamics, Vol. 37, No. 6 (2014), pp. 1984-1998, DOI: 10.2514/1.G000259

[53] Dang, Zh., Li, T., Wang, Zh., Zhang, Y., 2015, "Bounds on maximal and minimal distances for coplanar satellite relative motion under given initial conditions," Aerospace Science and Technology, No. 46, pp. 204-209, DOI: 10.1016/j.ast.2015.07.012

[54] Whipple, P. H ., 1970, "Some Characteristics of Coelliptic Orbits – Case 610," Bellcom Inc., Washington: NASA

[55] Fehse W., (chapter written by Ankersen, F.) "Appendix A: Motion Dynamics," *Automated Rendezvous and Docking of Spacecraft*, 1st ed., Cambridge University Press, Cambridge (UK), 2003, pp. 424-440, DOI: 10.1017/CBO9780511543388